

UC San Diego

UC San Diego Electronic Theses and Dissertations

Title

Hydrogen/deuterium-exchange (DXMS) analysis of the carbohydrate phosphatase, starch-excess 4

Permalink

<https://escholarship.org/uc/item/3bp082q0>

Author

Hsu, Simon

Publication Date

2008

Peer reviewed|Thesis/dissertation

UNIVERSITY OF CALIFORNIA, SAN DIEGO

**Hydrogen/Deuterium-exchange (DXMS) Analysis of the Carbohydrate Phosphatase,
Starch-excess 4**

A thesis submitted in partial satisfaction of the requirements for the degree

Master of Science

in

Biology

by

Simon Hsu

Committee in charge:

Professor Virgil L. Woods Jr., Chair
Professor Partho Ghosh, Co-Chair
Professor Amy Kiger

2008

The Thesis of Simon Hsu is approved and it is accepted in quality and form for
publication on microfilm and electronically:

Co-Chair

Chair

University of California, San Diego

2008

DEDICATION

Foremost, this is dedicated to my loving girlfriend, Rona. You are an incredible woman, always providing encouragement, support, and love. Through the busiest and hardest of times, you remain filled with spirit and optimism. Your cooking is divine.

I would also like to dedicate this to my family:

To my father, Jack, and my mother, Grace, for teaching me how to live.

To my brothers, Nelson and Joshua, and my sister, Emily, for filling my life with joy.

EPIGRAPH

“To avoid criticism do nothing, say nothing, be nothing.”

Elbert Hubbard

TABLE OF CONTENTS

Signature Page	iii
Dedication	iv
Epigraph... ..	v
Table of Contents	vi
List of Figures	vii
List of Tables.....	viii
List of Supplemental Figures.....	ix
Acknowledgements	x
Abstract	xi
Introduction	1
Materials and Methods	8
Results	12
Discussion	18
Figures and Tables.....	21
Supplemental Figures.....	34
References.....	80

LIST OF FIGURES

Figure 1: Exchangeable peptide hydrogens.....	21
Figure 2: Flow chart depicting automated protein processing and data analysis.....	22
Figure 3: Topography, conservation, and phylogeny of the domains of various DSPs.....	23
Figure 4: Representative partial model structures of glycogen and amylopectin.....	25
Figure 5: Pepsin-digested coverage map of high-quality apo- and amylopectin-bound SEX4 peptides.....	26
Figure 6: DXMS results for apo- and amylopectin-bound SEX4.....	27
Figure 7: Deuterium incorporation changes upon amylopectin binding.....	28
Figure 8: DSP binding site and acid loop show substrate-induced protection from solvent.....	29
Figure 9: AMPK β -GBD carbohydrate binding residues show substrate-induced protection from solvent.	31

LIST OF TABLES

Table 1: Biochemical characteristics of eukaryotic glycogen, amylopectin, and Lafora bodies.....	32
---	----

LIST OF SUPPLEMENTAL FIGURES

Supplemental Figure 1: Number of deuterons incorporated in amylopectin-bound and apo-SEX4 as a function of time for all 156 peptides obtained	34
Supplemental Figure 2: Deuterium incorporation changes upon amylopectin binding.	74

ACKNOWLEDGEMENTS

Those of us lucky enough to know Virgil L. Woods, Jr. know his passion for his work and for people. Whether in the laboratory or the medical clinic, his enthusiasm provides a source of inspiration for my own career goals. In addition to biochemical concepts, his support and guidance over the years have taught me life skills that cannot be read off a textbook. His intellectual and professional influence will follow me wherever I go. I am forever thankful.

I would also like to thank Dr. Partho Ghosh and Dr. Amy Kiger for being members of my committee.

Certainly, this thesis would not have been possible without Dr. Matthew S. Gentry. Thank you for providing frequent feedback throughout this project, and Eric Durrant for his frequent SEX4 purifications. I would also like to thank Jeramie Watrous for being one of my editors.

Last but not least, I'd like to thank all the members of Woods lab, especially Kyle Asmus, Sheng Li, and Tong Liu for their guidance and moral support.

ABSTRACT OF THE THESIS

Hydrogen/Deuterium-exchange (DXMS) Analysis of the Carbohydrate Phosphatase,
Starch-excess 4

by

Simon Hsu

Master of Science in Biology

University of California, San Diego, 2008

Professor Virgil L. Woods Jr., Chair

Lafora Disease (LD), a type of progressive myoclonus epilepsy, is a fatal autosomal recessive disorder. The hallmark of LD is the accumulation of insoluble polyglucosan deposits known as Lafora bodies in nerve, heart, liver, skin and skeletal muscle cells. Half of all LD cases are caused by mutations in the gene that encodes the dual specificity phosphatase, laforin. Laforin contains two domains: a carbohydrate-binding module (CBM) and a phosphatase domain. Together, they allow laforin to bind and dephosphorylate complex carbohydrates, an activity conserved from humans to plants. However, laforin has yet to be crystallized successfully, and the dynamic behavior of the two domains remains unknown.

Due to the unavailability of laforin for study, we probed solvent accessibility of the plant functional equivalent of laforin, starch-excess 4 (SEX4), utilizing enhanced

peptide amide hydrogen/deuterium (H/D) exchange mass spectrometry (DXMS) in order to elucidate the structural dynamics of these proteins. We also explored changes in H/D exchange of the SEX4 protein upon the binding of amylopectin, a glucose polymer and known substrate of both laforin and SEX4. Employing DXMS, we observed substrate-induced exchange decrease in regions of the CBM with conserved binding residues and in the phosphatase active site pocket. Exchange decrease was also observed in a loop of the CBM not implicated in carbohydrate binding, indicating a site undergoing substrate-induced allosteric changes or yet unidentified carbohydrate-binding residues. The lack of exchange rate changes in all other regions of SEX4 indicates that the phosphatase domain of SEX4 undergoes little conformational changes upon substrate binding, and likely retains an open and active conformation. The functional homology of SEX4 with laforin makes it highly likely our results hold true for laforin.

INTRODUCTION

1.1 Hydrogen/Deuterium Mass Spectrometry

The understanding of protein dynamics, structure, and conformational changes is essential for advancing our knowledge of human disease and guiding pharmaceutical drug design. Due to the idiosyncratic nature of proteins, it is often difficult or impossible to obtain data on these protein properties using current methods alone. Though techniques such as fluorescence spectroscopy and X-ray crystallography can observe protein-protein/substrate interactions, these methods provide limited details on protein dynamics, exhibit slow throughput, and require high (milligram) amounts of pure protein¹.

Peptide amide hydrogen/deuterium exchange mass spectrometry (DXMS) has emerged as a powerful method to study the elusive structurally dynamic characteristics proteins exhibit. Since a protein's structure and dynamics are critical for proper function, abnormal changes in these characteristics can compromise protein function and, in some instances, cell viability. Application of DXMS suggests mechanisms by which these proteins function during disease progression and can characterize the nature of pathological protein conformations. Automated high throughput, high resolution DXMS systems have been used to track structural changes in proteins implicated in numerous diseases including viral infections^{2,3}, blood coagulation^{4,5}, and lipid-mediated membrane binding^{6,7}. In this study, DXMS is applied to a protein functionally homologous to the one implicated in Lafora Disease.

1.2 Background and Theory of Hydrogen Exchange

Peptide amide hydrogens on the peptide backbone continuously and reversibly interchange with hydrogens in the surrounding solvent. By substituting solvent hydrogen with deuterium, a heavier isotope, the mass increase incorporated as a consequence of exchange at a specific location can be detected through mass spectrometry. The hydrogen-deuterium exchange rate, a function of both protein structure and solvent accessibility, provides valuable information about the structure and dynamics of a protein⁸.

Exchangeable hydrogens on proteins can be classified into three groups. Those found on the functional groups of amino acid side chains (-OH, -SH, NH₂, -COOH) exchange too rapidly to be measured, and do not retain deuterons during processing. The hydrogens attached directly to the α -carbon & side chain carbons are covalent and do not exchange. The hydrogens measurable by DXMS are those bonded to the amide nitrogens on the protein backbone (**Fig. 1A**) that have rates, under physiologic conditions, ranging from hundreds of milliseconds to years⁹.

For a particular amide hydrogen, local factors, such as steric blocking caused by neighboring amino acids, and solvent accessibility can affect the exchange rate. Amide hydrogens must make physical contact with the surrounding solvent for exchange to occur¹⁰. In a folded protein, hydrogens present in unstructured regions and lacking in hydrogen-bonding will have a rapid exchange rate on the order of seconds; those buried deep within a hydrophobic interior or involved in hydrogen-bonding will take days to months to fully exchange¹¹. Thus, amide hydrogen exchange rates provide information on the conformational properties of a folded protein.

1.3 Measuring H/D Exchange using Mass Spectrometry

There are two parts to a DXMS study: fragmentation tuning and deuterium on-exchange. During fragmentation tuning, the optimum conditions for proteolysis (e.g. denaturation conditions, flow rate over pepsin column) are determined. Undeuterated protein samples are added to “quench” buffers containing various concentrations of the denaturing salt guanidinium hydrochloride, rapidly proteolyzed to fragments ranging typically from 5-25 amino acids, and partially separated from each other by reverse-phase liquid chromatography to minimize overlap. To identify the pepsin-generated peptides for each digestion condition, a data-dependent data acquisition proceeds as a primary MS scan for parent mass identification, and MS/MS scans for peptide sequence identification are acquired. The data set is then analyzed via the SEQUEST database search algorithm to identify the sequence of the parent peptide ions and their chromatographic retention times. The conditions which yield the highest number of overlapping peptides with the most complete primary amino acid sequence coverage are subsequently employed for deuterium on-exchange sample preparation.

Deuterium on-exchange, performed under native conditions, measures the degree of deuterium uptake via the difference in peptide mass between pre- and post-incubation in D₂O buffer. Substrate-binding is predicted to mask regions from deuterium exchange by sterically blocking the bind site, and/or by altering protein structure or dynamics as to limit solvent exposure. To initiate the exchange reaction, a protein solution is incubated in an otherwise physiologic buffer supplemented in D₂O. At various time intervals, aliquots of the exchanging solution are “exchange quenched” by adjusting the pH to the combined minimum of acid (H⁺) and base (OH⁻) catalyzed exchange, ~ pH 2.5¹² (**Fig.**

1B), and lowering the temperature to 0 °C. Under quench conditions, loss of exchange-labeled deuterium from the protein peptide is greatly reduced, and deuterium-labeled peptides can now be subjected to mass spectrometry analysis and peptide identification utilizing the same process specified above. The masses of the deuterated peptides are then compared to the masses of the same peptides prepared from undeuterated protein. A map depicting regional levels of deuterium incorporation can be generated based on the various peptides. **Figure 2** outlines the automated protein processing and data analysis setup.

1.4 Lafora Disease

Lafora Disease (LD; OMIM #254780), a type of progressive myoclonus epilepsy, is a fatal autosomal recessive disorder that presents itself during adolescence, culminating in death a decade after onset¹³. LD is diagnosed by the presence of insoluble polyglucosan deposits termed Lafora Bodies (LBs) in neurons and other cell types in most organs^{14,15,16}, the accumulation of which is responsible for increased neuronal nonapoptotic cell death, myoclonic seizures, severe dementia, and death¹⁷. Approximately half of all LD cases are caused by recessive mutations in the EPM2A gene, encoding the protein laforin^{13,17}.

Laforin is a member of the dual specificity phosphatase family, which belongs to the protein tyrosine phosphatase (PTP) superfamily. All PTPs contain the signature HCXXGXXR active site motif¹⁸ and remove phosphates from phosphotyrosine substrates. Dual specificity phosphatases get their namesake because they can additionally dephosphorylate phosphoserine/phosphothreonine substrates⁴². Of all the phosphatases

in the animal kingdom, only Laforin possesses a carbohydrate-binding module (CBM, specifically type 20)¹⁹, located at the N-terminus. The other major domain in laforin is a C-terminal phosphatase active site (DSP; **Fig. 3A**). Together, these two domains give laforin the unique ability to liberate phosphates from complex carbohydrates (chains of three or more sugar molecules), whereas all other human phosphatases lack this activity¹⁹.

The molecular etiology of LD was a mystery until laforin's unique ability to liberate covalent phosphates on glycogen *in vivo* and *in vitro* was discovered²⁰. Glycogen, the main storage carbohydrate of mammals, is a glucose polymer that contains a small amount of covalently-linked phosphates, whose origin and function remain unsolved²⁰. Composed mostly of α -1,4 glycosidic linkages, glycogen will form an α -1,6 glycosidic linkage with another glucose every 12-14 glucose subunits (**Table 1; Fig. 4A**), resulting in a branching pattern that makes glycogen water-soluble. LBs have a backbone structure similar to glycogen, but have less ordered and fewer branches and are substantially more phosphorylated than glycogen. These biochemical features render LBs water-insoluble^{21,22}.

Laforin protein levels in murine models have been shown to increase with cytosolic glycogen concentration, and vice versa, which suggests laforin is a glycogen sensor that regulates its own production²². Furthermore, murine EPM2A knockout models have been demonstrated to exhibit excessively phosphorylated glycogen in liver and muscle tissue²⁰. These findings suggest that laforin removes phosphates during glycogen polymerization, and in its absence, hyperphosphorylated glycogen exhibits

decreased branching, resulting in LB formation. This model has since been supported by biochemical and patient data^{22,23}.

Despite the similarities between LBs and glycogen, biochemical studies characterize LBs as structurally more similar to the sugar amylopectin than any other compound, natural or synthetic²⁴. Amylopectin composes 75-90% of starch, the main storage carbohydrates in plants. Like glycogen, amylopectin forms α -1,4 glycosidic linkages, but branches discontinuously via α -1,6 glycosidic linkages every 12-20 residues, rendering it water-insoluble (**Table 1; Fig. 4B**). Amylopectin also has a higher phosphate content than glycogen making it more comparable to LBs. Overall, these studies show LBs and amylopectin as having near-identical characteristics.

At concentrations optimal for our DXMS studies (>4mg/ml), laforin forms undesirable inactive dimers *in vitro*. Fortunately, a functional equivalent of laforin, starch-excess 4 (SEX4), was discovered recently in plants¹⁷. Evolved independently, both laforin and SEX4 have been shown to efficiently liberate phosphates from the complex carbohydrate amylopectin, and are the only reported phosphatases in any kingdom with this activity^{17,19,20}. Mutations in the SEX4 gene result in starch-excess *Arabidopsis thaliana* mutants that accumulate starch, reminiscent of the LB phenomenon that characterize Lafora Disease^{25,26,27}. Similar to laforin, SEX4 contains a phosphatase domain and a CBM20-like carbohydrate-binding domain, though the domains of SEX4 are arranged in an opposite orientation (**Fig. 3B**)²⁸. The key HCX₂GX₂R motif that comprises the catalytic site of the phosphatase domain is present in both SEX4 and laforin. The presence of this motif, along with a phylogenetic search, shows SEX4 to be part of the dual specificity phosphatase family, with a 39% sequence similarity between

the DSPs of SEX4 and laforin¹⁷. However, a sequence search shows the CBM of SEX4 to be more similar to another class of CBM, the AMP-activated protein kinase β Glycogen Binding Domain (AMPK β -GBD).

Despite differences in sequence, both CBM20 and AMPK β -GBD domains interact with and bind individual glycan chains of carbohydrates. Furthermore, mutations in conserved carbohydrate binding residues present in the CBM20 of laforin and in the AMPK β -GBD of SEX4 impair their ability to dephosphorylate glycogen and amylopectin, respectively^{17,20}. In an elegant study, laforin has been shown to salvage the starch-excess phenotype in catalytically inactive SEX4 mutants¹⁷, thus solidifying the two phosphatases as functional equivalents.

DXMS has been widely used to analyze protein-ligand interactions^{29,30}, protein conformational changes³¹, and protein dynamics^{32,33}. The present study represents the first attempt to study SEX4 domain behavior and amylopectin binding effects. Our results suggest a possible allosteric change within the AMPK β -GBD upon substrate binding, though the two domains likely behave autonomously.

MATERIALS AND METHODS

2.1 Protein Expression and Purification

The SEX4 protein was provided by my collaborator, Dr. M. Gentry from the University of Kentucky. Since the first 81 amino acids of SEX4, which compose the bulk of a chloroplast-targeting protein (cTP, **Fig. 3B**), are highly hydrophobic and render the protein insoluble, we cloned and purified recombinant HIS-tagged Δ 81-SEX4. cTP-cleaved SEX4 has been shown to retain its catalytic activity and efficiently liberates phosphates from amylopectin¹⁷. HIS-tagged Δ 81-SEX4 was transferred into *Escherichia coli* cells of strain BL21 codon plus (DE3). The transformed cells were grown in a laboratory shaker at 37 °C in 2xYT until they reached an OD of 0.6 at 600nm. Protein expression was induced with IPTG overnight at room temperature and lysed in 100mM NaCl, 20mM Tris (pH 7.2), 3mM TCEP, and 5% (v/v) glycerol. The lysate was filtered by centrifugation at 19,000 rpms for 30 min and purified using a Profinia (Biorad) with Profinity IMAC 5ml cartridge (BioRad, #732-4614). The elute was concentrated to 10mg/ml, put over S75 sepharose GFC column, and concentrated with an Amicon 30k concentrator (Millipore) to 10 mg/ml.

2.2 Establishment of Optimal Proteolysis Conditions

At 0 °C, a 5 μ l sample of 10.0 mg/ml SEX4 protein in 20 mM Tris (pH 7.2), 100 mM NaCl, 3 mM TCEP, 5% (v/v) glycerol) was diluted with 15 μ l of 7.8 mM Tris (pH 7.1), 100 mM NaCl, mixed with 30 μ l of quench solution (containing either 0.08 M, 0.8 M, 1.6 M, 3.2 M, or 6.4 M guanidine hydrochloride in 0.8% (v/v) formic acid with 16.6% (v/v) glycerol), and transferred to dry ice within one minute of quench solution addition.

Vials with frozen samples were stored at $-80\text{ }^{\circ}\text{C}$ until transferred to the dry ice-containing sample basin of the cryogenic autosampler module of the DXMS apparatus. Temperature was controlled by keeping valves, tubing, columns, and autosampler within a refrigerator maintained at $4\text{ }^{\circ}\text{C}$, with columns immersed in melting ice. Samples were individually melted at $0\text{ }^{\circ}\text{C}$, then injected ($45\text{ }\mu\text{l}$) and pumped through a protease column (0.05% (w/v) trifluoroacetic acid (TFA) at $250\text{ }\mu\text{l}/\text{min}$, with 16 s exposure to protease) containing immobilized porcine pepsin (coupled to 20AL support from PerSeptive Biosystems at $30\text{ mg}/\text{ml}$; $66\text{ }\mu\text{l}$ column bed volume). Protease-generated fragments were collected on a C18 HPLC column, and eluted by a linear acetonitrile gradient (5% - 45% (v/v) solvent B in 30 min at $50\text{ }\mu\text{l}/\text{min}$. Solvent A was 0.05% TFA in water; solvent B was 80% (v/v) acetonitrile, 20% water, 0.01% TFA) and injected directly into the mass spectrometer with data acquisition in either MS1 profile mode or data-dependent MS/MS mode. The column effluent was analyzed on an LCQ Classic (Thermo Finnigan Inc.) electrospray ion trap-type mass spectrometer with capillary temperature at $200\text{ }^{\circ}\text{C}$ and an electrospray Q-TOF mass spectrometer (Micromass). Fragmentation maps that visually overlay proteolyzed peptide fragments over the protein primary amino acid sequence for all concentrations of denaturant were generated. It was found that 0.08 M guanidine hydrochloride quench solution (final concentration of 0.05 M guanidine hydrochloride) gave the most complete coverage with densely overlapping peptides and was used in all subsequent experiments.

2.3 On-exchange Protein Deuteration

After establishment of the fragmentation maps, exchange-deuterated samples of SEX4 were prepared and processed following the procedure described above, except that 5 μ l of each protein stock solution was diluted with 15 μ l of Deuterium Oxide (D_2O) buffer, containing 7.8 mM Tris, 10 mM NaCl, pD (read) 7.1. In sugar-binding experiments, the SEX4 in protein buffer was pre-incubated in the presence of 5 mg/ml amylopectin (Sigma 10118) at room temperature for 30 min and then chilled to 0 $^{\circ}C$. The ice-cold D_2O buffer was then added, and the samples were incubated in the cold-room on ice for 10 s, 100 s, 300 s, 1000 s, 3000 s, 10,000 s, 30,000 s, 100,000 s, 300,000 s, then mixed with 30 μ l of quench solution (0.8% (v/v) formic acid, 0.08 M guanidine hydrochloride, 16.6% (v/v) glycerol), transferred to ice-cooled autosampler vials, frozen on dry ice, and stored at $-80^{\circ}C$. Non-deuterated and equilibrium-deuterated samples were prepared for comparison by the addition of 5 μ l SEX4 (8.5 mg/ml, 20 mM Tris (pH 7.2), 100 mM NaCl, 3 mM TCEP, 5% (v/v) glycerol) to either 15 μ l of 7.8 mM Tris (pH 7.1), 100 mM NaCl on ice (non-deuterated sample) or to 15 μ l 0.5% formic acid in D_2O overnight at room temperature (equilibrium deuterated sample). Quench was performed with 30 μ l of quench solution as described above. Data for the deuterated sample sets were acquired in a single automated 8 h run with Q-TOF analysis only. Subsequent data reduction was performed with the DXMS data reduction software as described below.

2.4 Data Processing

The SEQUEST program (Thermo Finnigan Inc.) was used to identify the likely sequence of the parent peptide ions and these tentative identifications were tested with

specialized DXMS data reduction software developed in collaboration with Sierra Analytics, LLC, Modesto, CA. All selected peptides first passed the quality control threshold established by the software and were then manually checked for the mass envelope fitting with the calculated mass envelope for data reduction. The highest signal/noise ion was picked if multiple ionization charges (1, 2, or 3) of a peptide were detected. Normally, the peptide with the lowest charge state gave the best signal. To correct for the loss of exchange-labeled deuterium on peptides that “back-exchange” to hydrogen during processing, the following equations were used to determine deuteration level and deuterium incorporation for each peptide³⁴:

$$\text{Deuteration Level (\%)} = \frac{m(P) - m(N)}{m(E) - m(N)} \times 100\%$$

$$\text{Deuterium incorporation (number)} = \frac{m(P) - m(N)}{m(E) - m(N)} \times \text{MaxD}$$

$m(P)$, $m(N)$, and $m(E)$ are the centroid values of a partially deuterated peptide, non-deuterated peptide, and equilibrium deuterated peptide, respectively. MaxD is the maximum deuterium incorporation calculated by subtracting the number of proline residues in the third or later amino acid residue and two from the number of amino acid residues in the peptide of interest (assuming the first two amino acid residues back-exchange too rapidly to retain deuterons⁴⁵).

RESULTS

3.1 SEX4 Coverage Map of Pepsin Fragmentation

The ability to localize and quantify detailed hydrogen exchange behavior with DXMS is largely determined by the sequence coverage and density of the proteolyzed peptide fragments produced and identified. The optimized condition for this protein, 0.05M guanidine hydrochloride and 250ul/min flow rate over the pepsin column (66ul bed volume) produced 156 high-quality peptides found in both the apo- and amylopectin-bound SEX4, and covered the entire sequence (307 aa) of the HIS-tagged Δ 81-SEX4 construct (**Fig. 5**). Results obtained with twenty-seven of the 156 peptides, chosen for their short length, are reported in this manual. The remaining 156 peptides in overlapping regions exhibited exchange behavior concordant to the twenty-seven reported (**Supp. Fig. 1**).

3.2 Binding Sites Show Preferential Solvation

DXMS was used to investigate the structural properties of SEX4 in solution and to provide a control to which subsequent experiments with bound amylopectin could be compared. The DXMS profile of apo-SEX4 is shown in the top set of colored bars in **Figure 6**, where unresolved amino acid residues are due to the fact that the first residue of each peptide lacks an amide hydrogen, and the first N-terminal amide of each peptide exchange too rapidly to retain deuterons during processing⁴⁵.

Within the DSP of all dual specificity phosphatases are three functionally important regions: the D-loop (or general acid loop), the HCX₂GX₂R motif, and the “variable” loop (**Fig. 8A**). Together, the D-loop and HCX₂GX₂R motif compose the

catalytic site. Asp 166 in the D-loop functions as a general acid/base catalyst, allowing Cys 198 in the HCX₂GX₂R motif to nucleophilically attack the phosphorus atom of the phosphate moiety and dephosphorylate the substrate³⁵. The variable loop is largely responsible for the architecture of the active site pocket, and assists in orientating the HCX₂GX₂R Arg to interact with the target phosphate⁴². Interestingly, the variable loop and the D-loop are the two most rapidly deuterated regions in the DSP (**Fig. 6**), indicating a high degree of solvent exposure. The peptide covering the HCX₂GX₂R motif stops short of maximal deuteration at the longest incubation time point (300,000 s), but achieves the highest deuteration level of all peptides within the DSP at the 10 s time point, similarly indicating high solvent accessibility.

The AMPK β -GBD of SEX4 contains five putative carbohydrate binding residues (W278, K307, W314, G329, N333)^{36,37} conserved in the AMPK β -GBD family, mutations in which impair the ability of SEX4 to bind and dephosphorylate amylopectin¹⁷. The peptides containing a majority of these carbohydrate binding residues (all except K307) achieve the highest deuteration level of all peptides within the AMPK β -GBD at the 10 s time point. Cumulatively, these data suggest that the accessibility of the catalytic site, active site pocket, and carbohydrate binding site is likely to be important for substrate binding and enzymatic action. To further characterize the structural dynamics of SEX4 and how it binds and dephosphorylates complex carbohydrates, we probed the solvent accessibility of the SEX4 protein in complex with amylopectin.

3.3 Binding Sites Protected in Amylopectin-SEX4 Complex

The DXMS profile of amylopectin-bound SEX4 is shown in the bottom set of colored bars in **Figure 6**. To localize substrate-bound deuteration changes precisely, we determined the deuterium incorporation for each peptide over the nine time points (**Supp. Fig. 1**) and calculated the changes between the amylopectin-bound and apo-SEX4 at each time point (**Supp. Fig. 2**). Comparisons of deuterium incorporation into amylopectin-bound and apo-SEX4 reveal no instances of significant substrate-induced deuteration increase (>10%) at any time point anywhere in the protein (**Supp. Fig. 2**). Dramatic substrate-induced decreases (>10%) however were observed (**Fig. 7**), and mapped onto homologous structures (**Figs. 8 & 9**). Substrate-induced decreases (>10%) within the DSP were localized to peptides in the variable loop and the D-loop peptide (**Fig. 8**). Interestingly, in the absence of substrate these two regions are the two most rapidly deuterated regions in the DSP, signifying extensive interactions between the SEX4 protein and the amylopectin in solution in these regions.

Residues 313-333 of the AMPK β -GBD contains 3 of the 5 implicated binding residues, and are immediately blocked from solvent exposure upon amylopectin binding (**Supp. Fig. 2, 10 s**). In the absence of substrate, this region is similarly the most rapidly exchanging peptide in the AMPK β -GBD (**Fig. 6**). With increasing time, peptides containing the other 2 implicated binding residues exhibit significantly decreased deuteration levels (**Fig. 9**). Additionally, a loop in the AMPK β -GBD without implicated binding residues (residues 262-275) also shows significant substrate-induced exchange decrease (**Fig. 9**). Slowed amide exchange within this region suggest that amylopectin

binding triggers allosteric changes in structure that reduce the dynamics of this loop, which is located outside of the carbohydrate-binding site. Mutations in the putative carbohydrate-binding residues have been shown to completely abolish glycogen binding, but minimally affect the phosphatase activity of SEX4¹⁷. This indicates neither substrate-binding nor the substrate-induced allosteric change triggers the phosphatase activity of the SEX4 DSP, revealing the two domains are likely acting independently. Interestingly, this region maps to the same face as the carbohydrate-binding site on our 3D homology model. Since mutagenesis studies have not been performed on any of the residues in this region, including 3 highly conserved residues among the AMPK β -GBD family (G265, V269, G273)^{36,37}, the possibility of yet unidentified residues within this region that assist in carbohydrate binding cannot be ignored.

Finally, there are no changes evident in all other regions of the SEX4 protein, including the ~15 amino acid junction between the two domains (**Supp. Fig. 1, peptide 236-247**). Altogether, these observations indicate SEX4 is a carbohydrate phosphatase whose DSP likely adopts an open conformation that remains active regardless of whether or not substrate is bound to the AMPK β -GBD. Though the DSP does not undergo major conformational changes upon substrate binding, the previously mentioned loop in the AMPK β -GBD located outside known amylopectin contact regions may experience allosteric changes.

3.4 Implications for Catalysis

Our model supports the catalytic desphosphorylation mechanism exhibited by protein tyrosine phosphatases³⁵, and the modus operandi of CBM-containing enzymes,

which typically target a specific type of carbohydrate and modify it through enzymatic action³⁸. The deuteration decreases observed within the SEX4 AMPK β -GBD suggest it binds amylopectin with the 5 putative binding residues, which positions the carbohydrate for dephosphorylation by the DSP. The variable loop pocket, an implicated binding site, also helps orient the HCX₂GX₂R Arg to coordinate two of the phosphoryl oxygen atoms for proper phosphate removal³⁵. The D-loop Asp functions as an acid/base catalyst, where the HCX₂GX₂R Cys nucleophilically attacks the phosphorous atom of the substrate phosphate. The deuteration decreases observed within the DSP reflect solvent blockage that occurs as a result of these processes.

3.5 Comparison with the phosphoinositide phosphatase MTMR2

Similar DXMS experiments performed on a phosphoinositol-binding dual specificity phosphatase, the myotubularin MTMR2, yielded comparable results³⁹. MTMR2, like SEX4 and laforin, is part of a unique subgroup of dual specificity phosphatases that dephosphorylate nonproteinaceous substrates (**Fig. 3E**). MTMR2 has a similar domain organization compared to SEX4 and laforin, with a substrate-binding domain, the PH-GRAM domain, and a DSP. DXMS results for apo-MTMR2 reveal a highly solvent accessible active site pocket, highly solvent accessible PI-binding loops, and a poorly solvent accessible substrate-binding/phosphatase domain junction region. All these characteristics are observed in our apo-SEX4 results. PI-bound MTMR2 similarly show a dramatically decreased rate of exchange within its variable loop and no other changes evident in all other regions of the protein, including the PH-GRAM/phosphatase domain junction. The lack of change in the PH-GRAM domain that

would indicate substrate binding was attributed to the characteristic low affinity binding exhibited by the majority of PH domains. Based on these results existing domain/domain interactions in MTMR2 was determined to remain unaltered upon substrate binding. Our SEX4 studies show similar results, in addition to substrate-induced deuteration decreases in a region (residues 262-275) not known to contact amylopectin. Identifying this region as a substrate contact region would similarly indicate a lack of change in existing intra-domain interactions upon carbohydrate binding. Whether this possibility, or an allosteric change is responsible for the substrate-induced decrease, remains to be determined. This can be achieved through mutagenesis studies.

DISCUSSION

The lack of crystal structures for both laforin and SEX4 lead my collaborator, Dr. M. Gentry to suggest using the crystal structures of the tumor suppressor, phosphate tensin homologue (PTEN) DSP and *Homo sapiens* AMPK β -GBD as tentative structural models for the SEX4 DSP and CBM, respectively. An evolutionary phylogeny using Phylip clusters PTEN with SEX4 and laforin, showing they are part of a subgroup of DSPs that uniquely dephosphorylate nonproteinaceous substrates^{17,40} (**Fig. 3E**). The CBM of SEX4, classified in the AMPK β -GBD subclass, naturally exhibits a similar sequence and predicted 2° structure with that of *Homo sapiens* AMPK β -GBD (**Figs. 3D & 6**). PTEN, also part of the dual specificity phosphatase family, likewise contains the signature HCX₂GX₂R motif and a similar predicted 2° DSP structure to the DSP of SEX4 (**Figs. 3C & 6**), but has a relatively low degree of sequence similarity with SEX4 or laforin outside this motif⁴¹. Despite this fact, the DSP of PTEN exhibits a very similar three-dimensional structure to those of the DSPs of other dual specificity phosphatases solved so far, a family of phosphatases known to share the same tertiary structure⁴².

Our apo-SEX4 analyses reveal the highly solvent accessible nature of most of the putative carbohydrate binding residues (all except K307) within the AMPK β -GBD, evident by the high deuteration level after the 10 s time point. Substrate-binding residues located on the protein surface contact the deuterated solvent and will undergo rapid hydrogen/deuterium exchange (within seconds⁴³). As such, the 10 s duration is sufficient to selectively deuterate the most solvent-accessible amides^{44,45}. Lys 307, the only binding residue not to exhibit a high deuteration level after 10 s is unlike the other four putative binding residues in that it maps to a non-surface-exposed region buried within

the AMPK β -GBD on the homologous structure (**Fig. 8**). This reason may account for the fact that deuteration decrease in residues 307-313 remains unobserved until the latest time points (10,000 s through 300,000 s).

Residues 262-275, whose function in carbohydrate-binding remains unclear, were observed to undergo possible substrate-induced allosteric changes that result in a decreased H/D exchange rate. Since this region maps onto the same face as the carbohydrate-binding site on the homologous structure, yet unidentified residues that assist in carbohydrate binding may exist in this region. In previous studies that aimed to identify residues necessary for carbohydrate binding, a few highly conserved residues in proteins of the AMPK β -GBD family were selected for mutagenesis studies based on sequence alignment with related glycogen or starch binding domains and homology models^{36,37}. None of the residues in this region, including the highly conserved G265, V269, G273 have been targets of mutagenesis studies.

All of the regions within apo-SEX4 that are the most solvent accessible (the variable loop, D-loop, and surface-exposed carbohydrate binding residues within the AMPK β -GBD) are regions that exhibit significant protection from solvent upon amylopectin binding. The accessibility of the variable loop would facilitate insertion of the phosphorylated amylopectin into the catalytic site, allowing the D-loop to catalyze the dephosphorylation reaction. Substrate-induced structural changes within the DSP are shown not to propagate outside of these regions, indicating that the DSP is likely always in an open and active conformation. Consistent with this conclusion is the fact that mutations in the putative carbohydrate binding residues in the AMPK β -GBD minimally affect the phosphatase activity of SEX4¹⁷. Accordingly, the two domains can be said to

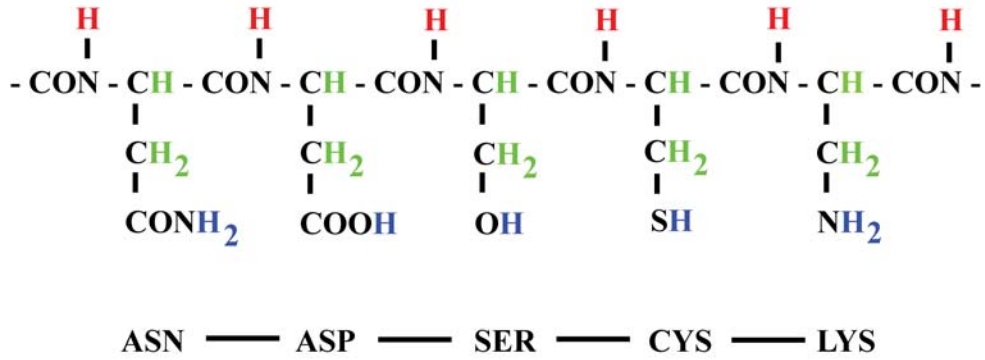
act autonomously. Mutations in the putative binding residues do, however, reduce the ability of SEX4 to dephosphorylate amylopectin¹⁷, which suggests it is the position of the bound carbohydrate, and therefore the position of the AMPK β -GBD relative to the DSP that is important for the ability of SEX4 to dephosphorylate its substrate¹⁷.

Finally, residues 101-129, adjacent to the variable loop in the DSP domain are strikingly solvent inaccessible even after the longest time point (300,000 s; **Fig. 6**). Based on this observation, it could be likely that the AMPK β -GBD is positioned near or atop this loop, preventing amide hydrogens from being solvated, regardless of the substrate binding status of SEX4.

We have described the results of structural analyses of the carbohydrate-specific dual specificity phosphatase, SEX4, in complex with amylopectin. The functional equivalence of SEX4 with laforin *in vivo* and similar behavior *in vitro* make it extremely likely that our results for SEX4 will hold true for laforin. Collectively, these results suggest that SEX4 and laforin are indeed carbohydrate phosphatases, but a crystal structure will be needed for a definitive answer. To this end, truncation of the heavily deuterated trailing SEX4 cTP residues and the C-terminus of the AMPK β -GBD (**Fig. 6**), which contain no predicted functional domains, may be required for successful crystallization of SEX4 and laforin.

FIGURES AND TABLES

A



B

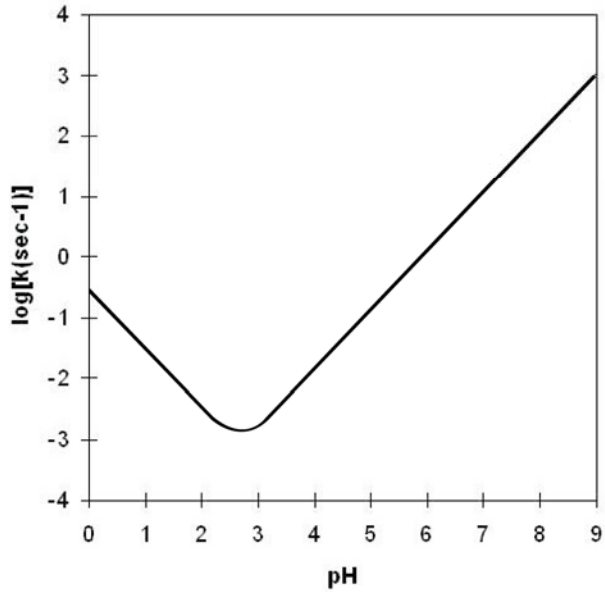


Figure 1. (A) Exchangeable peptide hydrogens. Red “amide hydrogens” are measurable by DXMS. Green “carbon hydrogens” are covalently bonded to carbon and do not exhibit exchange. Blue “side chain hydrogens” do not retain deuterons during processing due to their rapid exchange rates. (B) Peptide amide exchange rate constant vs. pH.

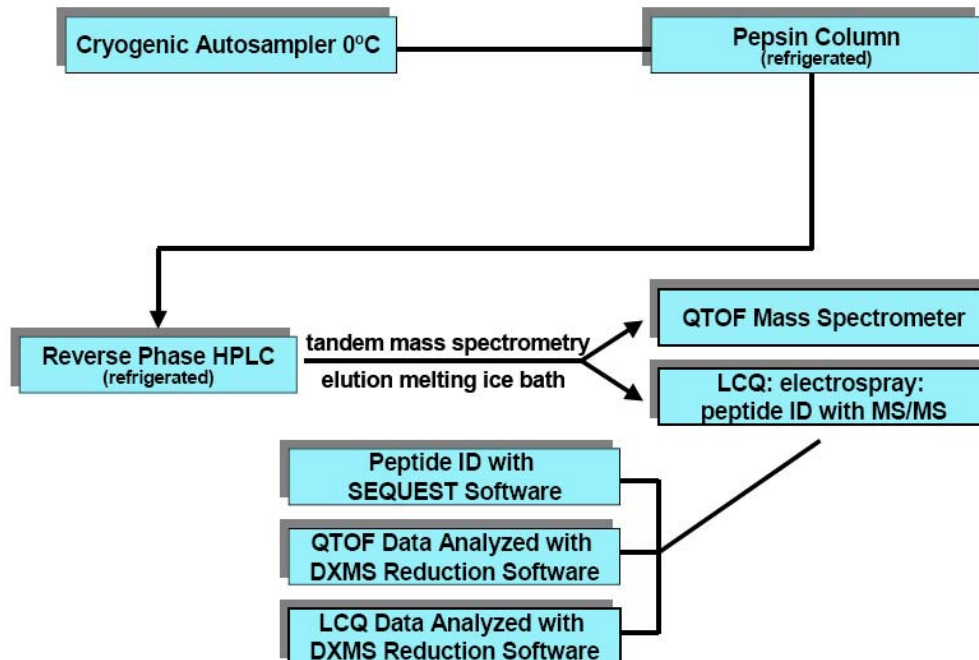
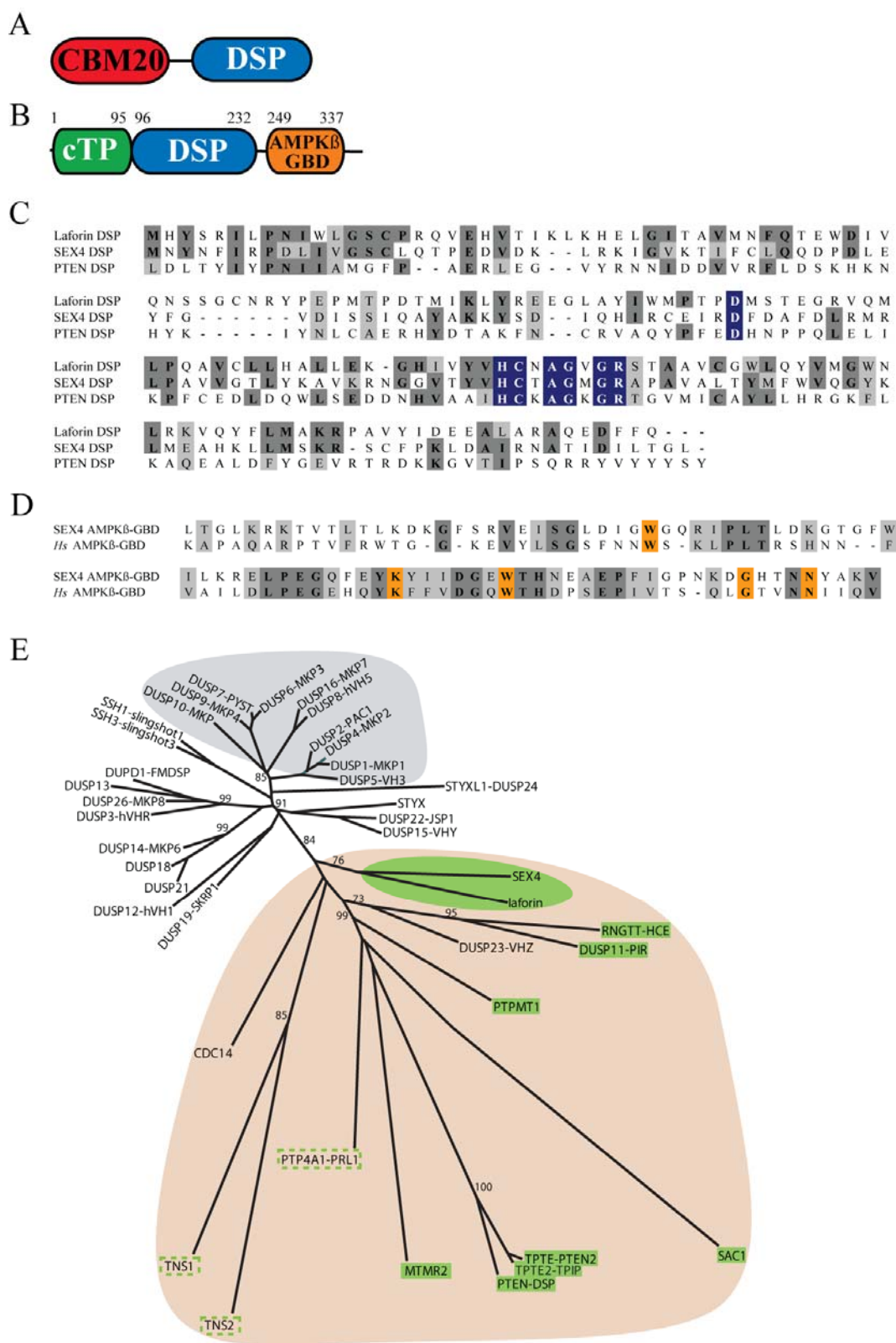


Figure 2. Flow chart depicting automated protein processing and data analysis.

Figure 3. Topography, conservation, and phylogeny of the domains of various DSPs. (A) Laforin and (B) SEX4 domain organization; CBM20 = carbohydrate binding module class 20; DSP = dual specificity phosphatase; cTP = chloroplast-targeting protein; AMP-activated protein kinase β Glycogen Binding Domain (AMPK β -GBD). (C) Alignment of the DSPs of laforin, SEX4, and PTEN (ClustalW). Residues boxed in blue are part of the DSP catalytic site, those boxed in dark gray are identical, and those boxed in light gray are conserved substitutions. (D) Alignment of the AMPK β -GBDs of SEX4 and *Homo sapiens* AMP-activated protein kinase (*Hs* AMPK β -GBD). Residues boxed in orange mark residues necessary for carbohydrate binding, those boxed in dark gray are identical, and those boxed in light gray are conserved substitutions. (E) Phylogeny of all DSP phosphatase domains (Phylip) generates 3 distinct clusters: evolutionarily recent “classical” DSPs (grey), and two clusters of the more ancient and divergent “atypical” DSPs (uncolored and tan). Interestingly, many DSPs within the atypical group that includes laforin (tan) have been proven to desphosphorylate non-proteinaceous substrates (phosphoinositols, RNA; green highlights) while others have suspect substrates and/or have activity against non-proteinaceous substrates *in vitro* (green dashed line).



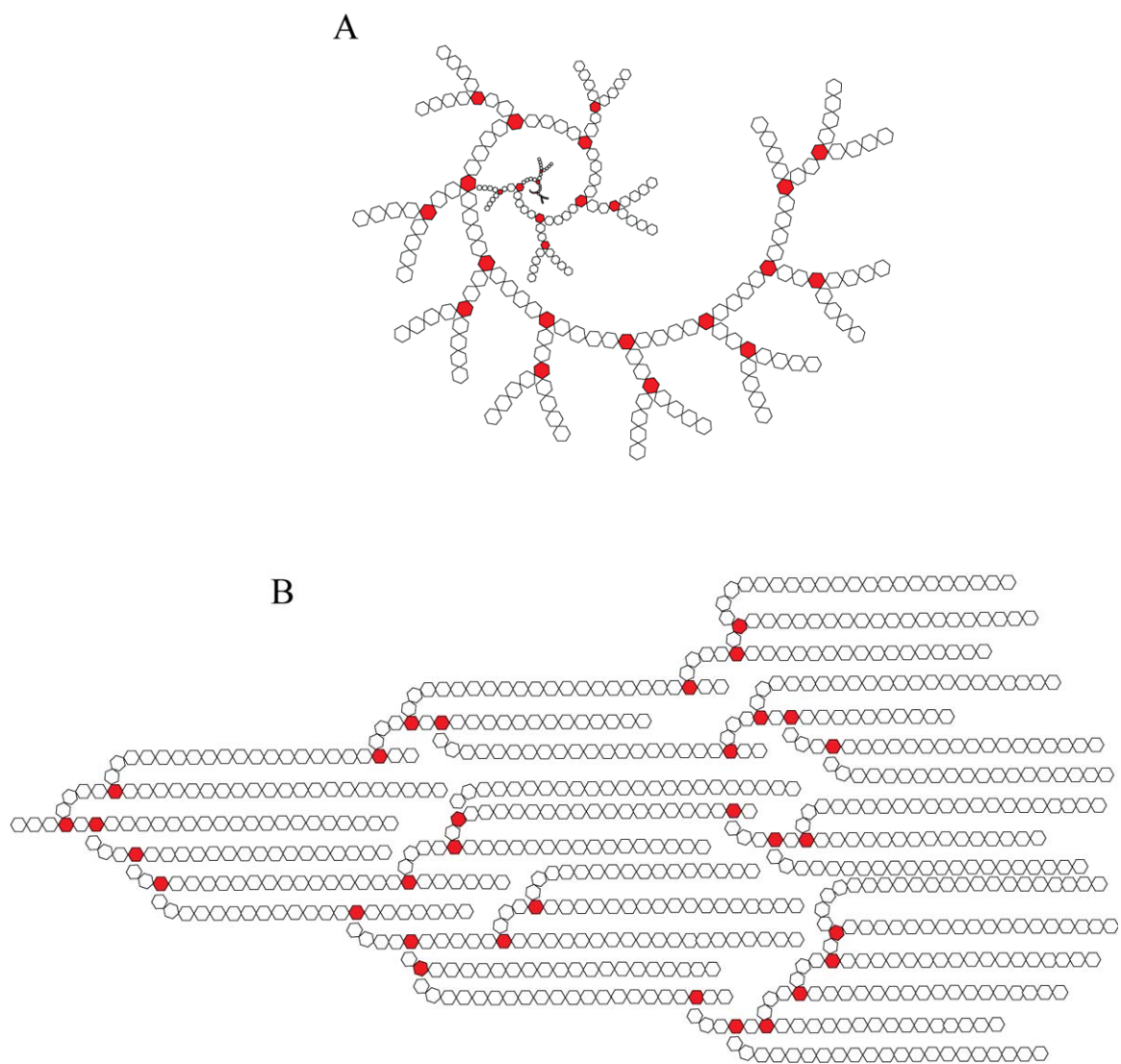


Figure 4. Representative partial model structures of (A) glycogen and (B) amylopectin. Colorless hexagon units denote α -1,4 linked D-glucose. Red hexagon units denote α -1,4,6 linked D-glucose branchpoints.

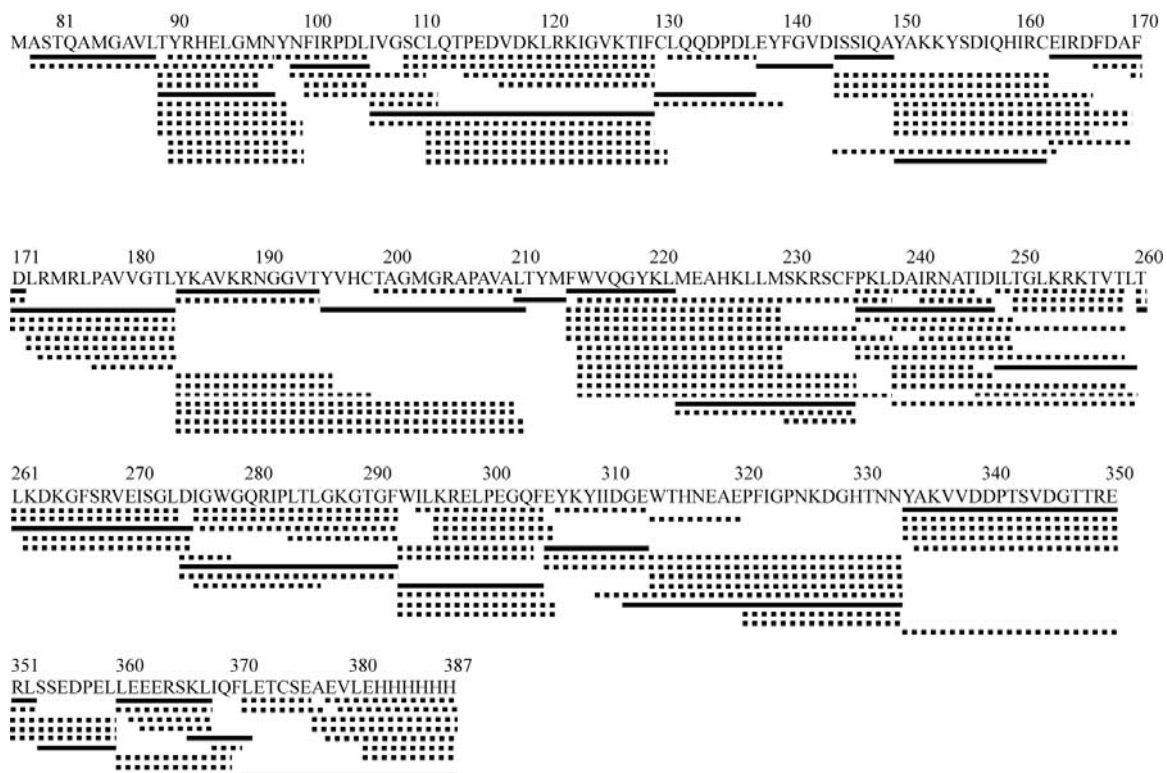


Figure 5. Pepsin-digested coverage map of high-quality apo- and amylopectin-bound SEX4 peptides. Peptides shown as solid lines were used in this study.

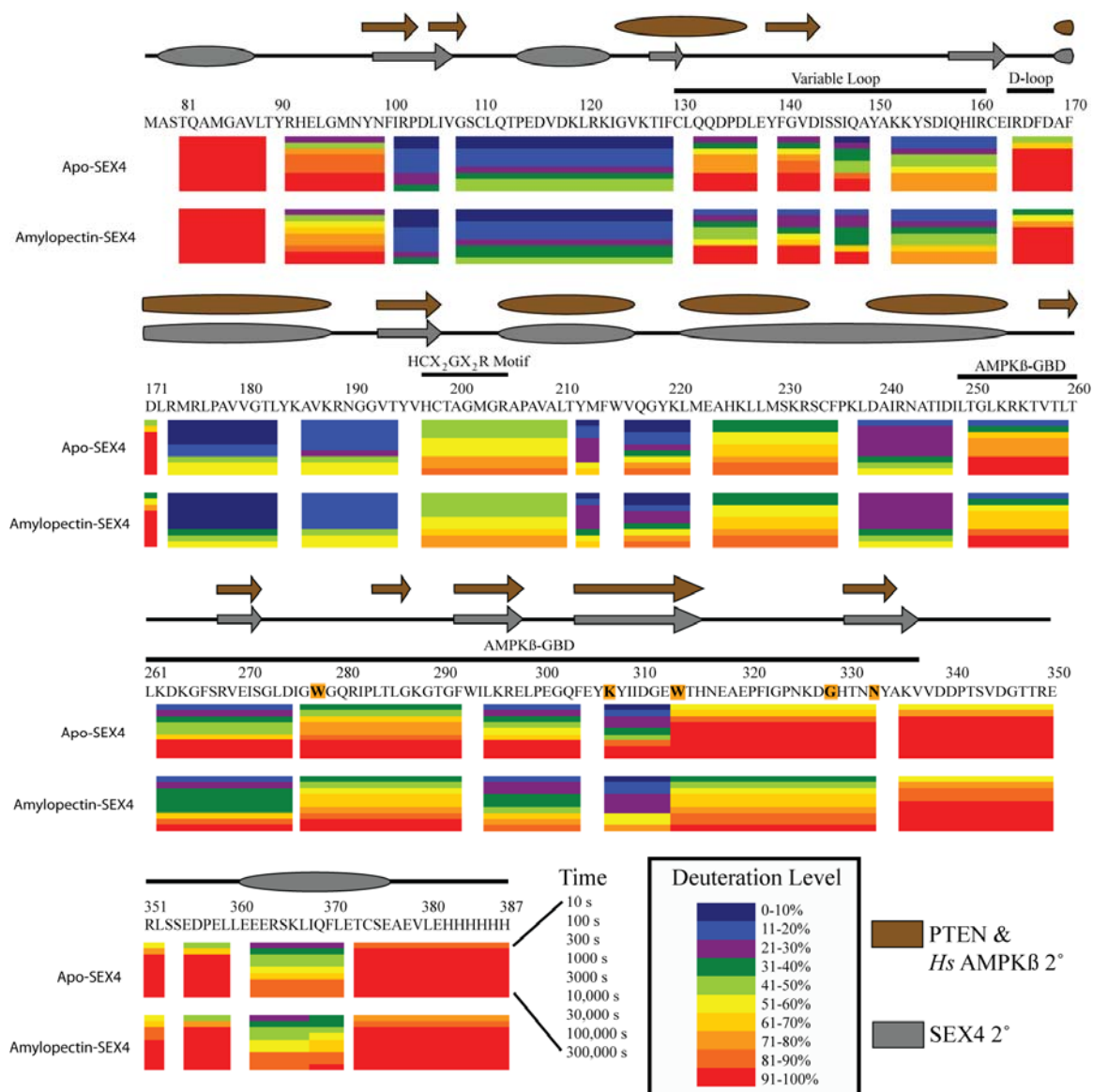


Figure 6. DXMS results for apo- and amylopectin-bound SEX4. The top set of colored bars corresponds to apo-SEX4. The bottom set, for amylopectin-bound SEX4. The bars, representing peptides, are divided into rows, each representing the percent deuteration at one of nine time points ranging from 10 s to 300,000 s (83 hr). Predicted secondary structural elements (PSI-PRED) are shown above the primary sequence (α -helices as arrows, β -pleated sheets as ellipses). Predicted secondary structure of the phosphatase domain of PTEN & the glycogen binding domain of *Homo Sapiens* AMP activated protein kinase (*Hs* AMPK β -GBD) is shown in brown, and that of SEX4 is gray. Regions of importance are also labeled above the primary sequence they cover. Residues highlighted in orange are implicated carbohydrate binding residues^{36,37}.

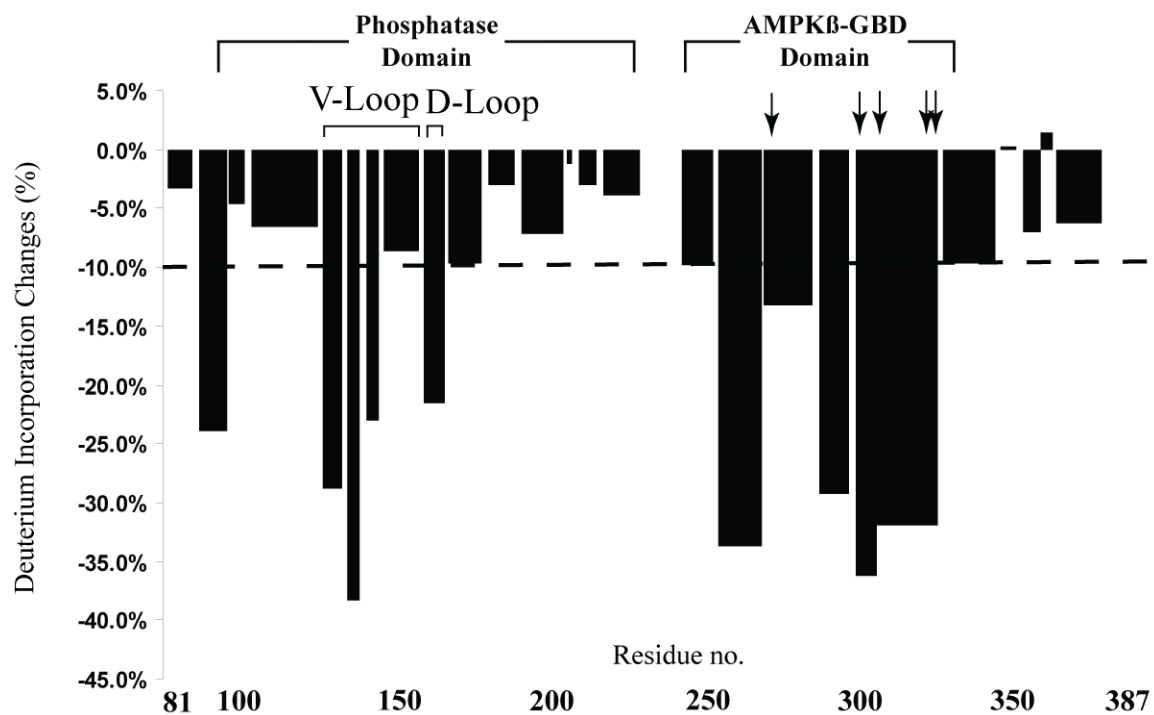
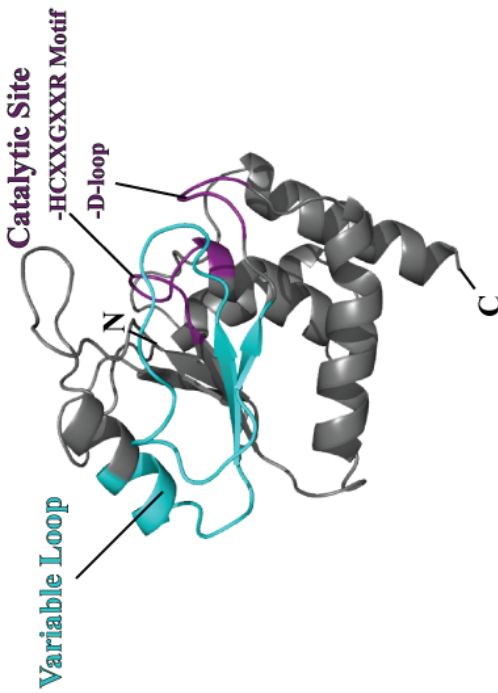


Figure 7. Deuterium incorporation changes upon amylopectin binding. A positive value indicates increased deuteration, and a negative value indicates decreased deuteration after amylopectin binding. Changes greater than 10% (broken line) are considered to be significant. This graph is a composite of the residues that showed the greatest negative deuteration change at any time point (**Supp. Fig. 2**) V-loop = Variable loop. Arrows indicate putative key carbohydrate binding residues (from left to right: W278, K307, W314, G329, N333)

Figure 8. DSP binding site and acid loop show substrate-induced protection from solvent. (A) Variable loop (teal) and catalytic site (dark purple) on PTEN DSP structure. (B) Number of deuterons incorporated as a function of time for selected residues in amylopectin-bound (purple) and apo- (blue) SEX4. Binding-induced deuterium incorporation changes within the DSP from **Figure 7** are mapped onto the PTEN DSP structure. The most rapidly deuterated regions in apo-SEX, the variable loop and catalytic site show significantly decreased exchange upon amylopectin binding. Residues on the structure with no data are represented in gray. Figure was created using pymol (DeLano Scientific, South San Francisco, CA; <http://pymol.sourceforge.net>)

PHOSPHATASE DOMAIN

A



B

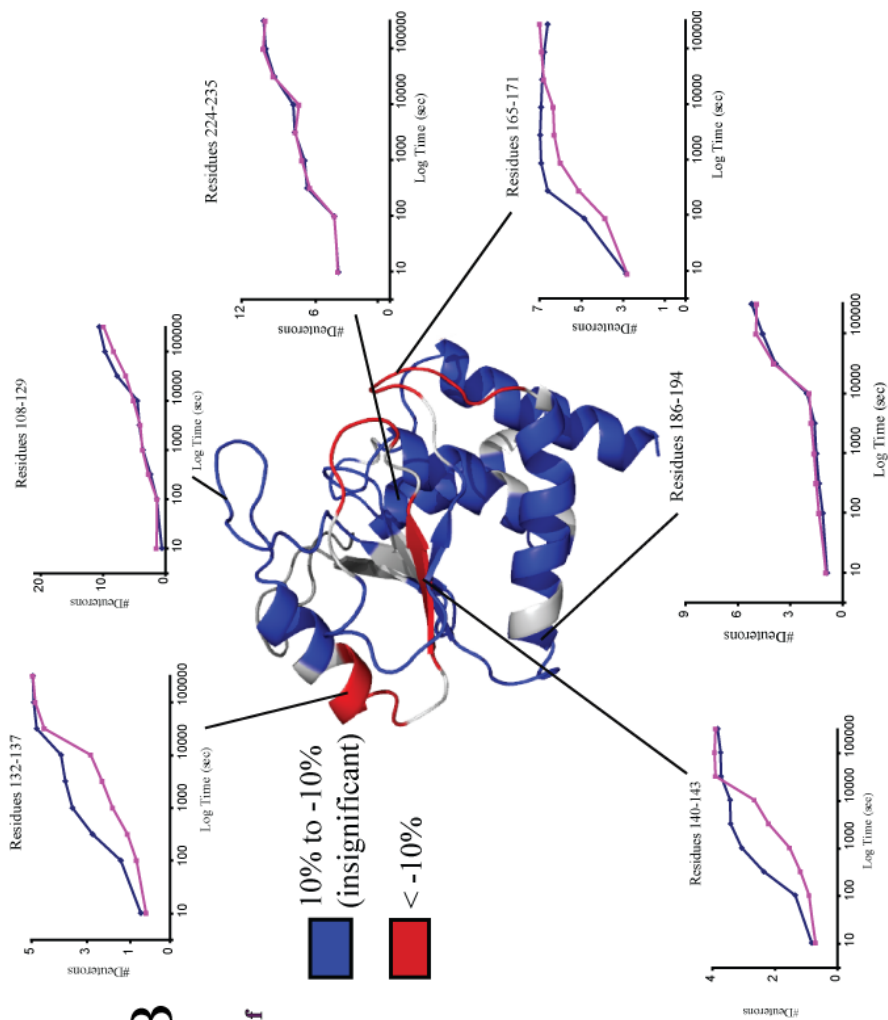
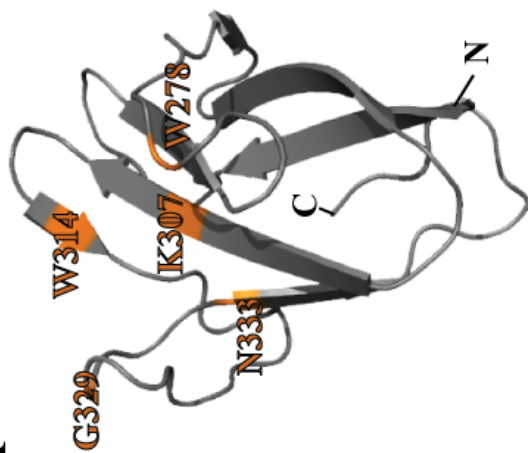


Figure 9. AMPK β -GBD carbohydrate binding residues show substrate-induced protection from solvent. (A) Five implicated carbohydrate binding residues on the *Homo Sapiens* (*Hs*) AMPK β -GBD structure. (B) Number of deuterons incorporated as a function of time for selected residues in amylopectin-bound (purple) and apo- (blue) SEX4. Binding-induced deuterium incorporation changes within the AMPK β -GBD from **Figure 7** are mapped onto the *Hs* AMPK β -GBD structure. The most solvent accessible binding residues in apo-SEX4 – W278, W314, G329, N333, – are surface-exposed, and are the most rapidly protected upon amylopectin binding. K307, located in a region of slower exchange in apo-SEX4, is not surface-exposed, and shows no significant decrease at 300 s. However, it is significantly protected at the later time points. Residues 262-275, whose function in carbohydrate-binding remain unclear, may be a site of substrate-induced allosteric change or contain unidentified carbohydrate-binding residues. Residues on the structure with no data are represented in gray.

AMPK β -GBD

A



B

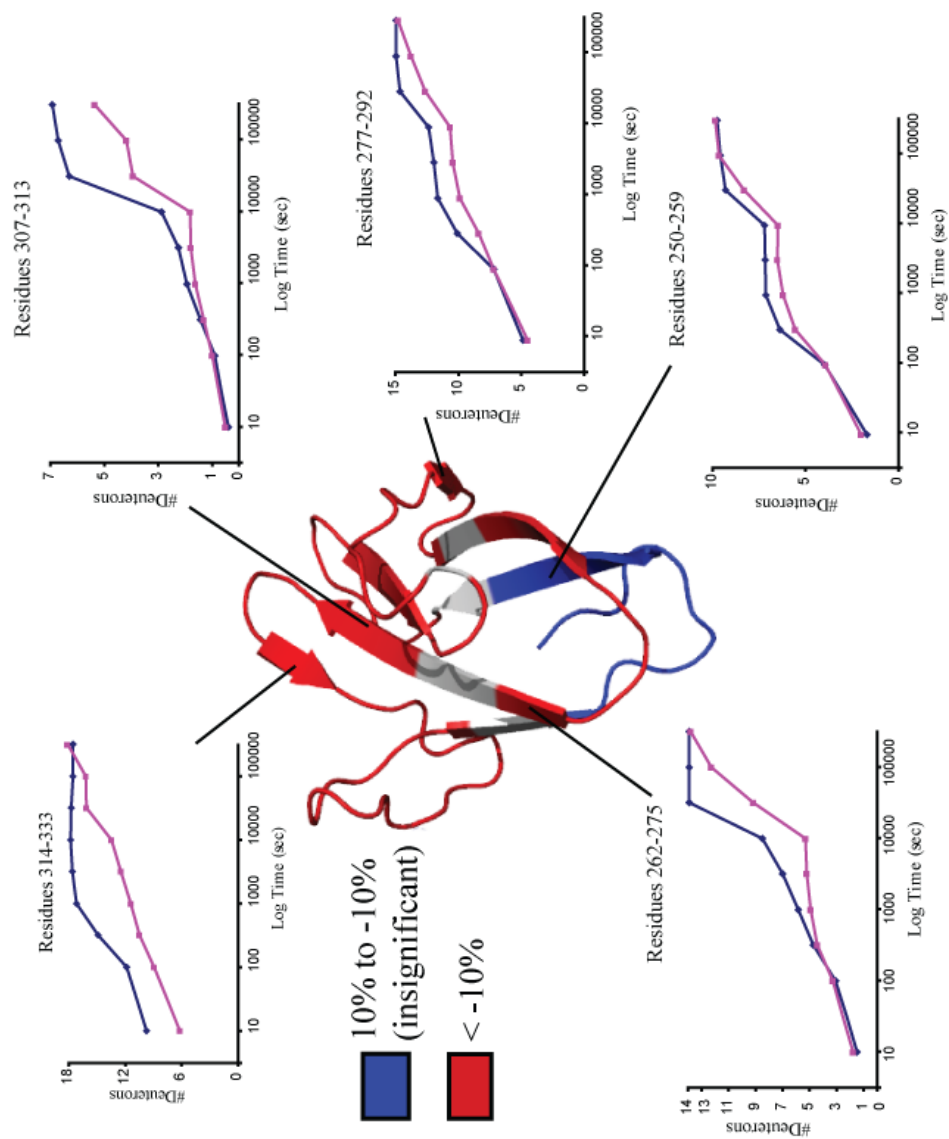
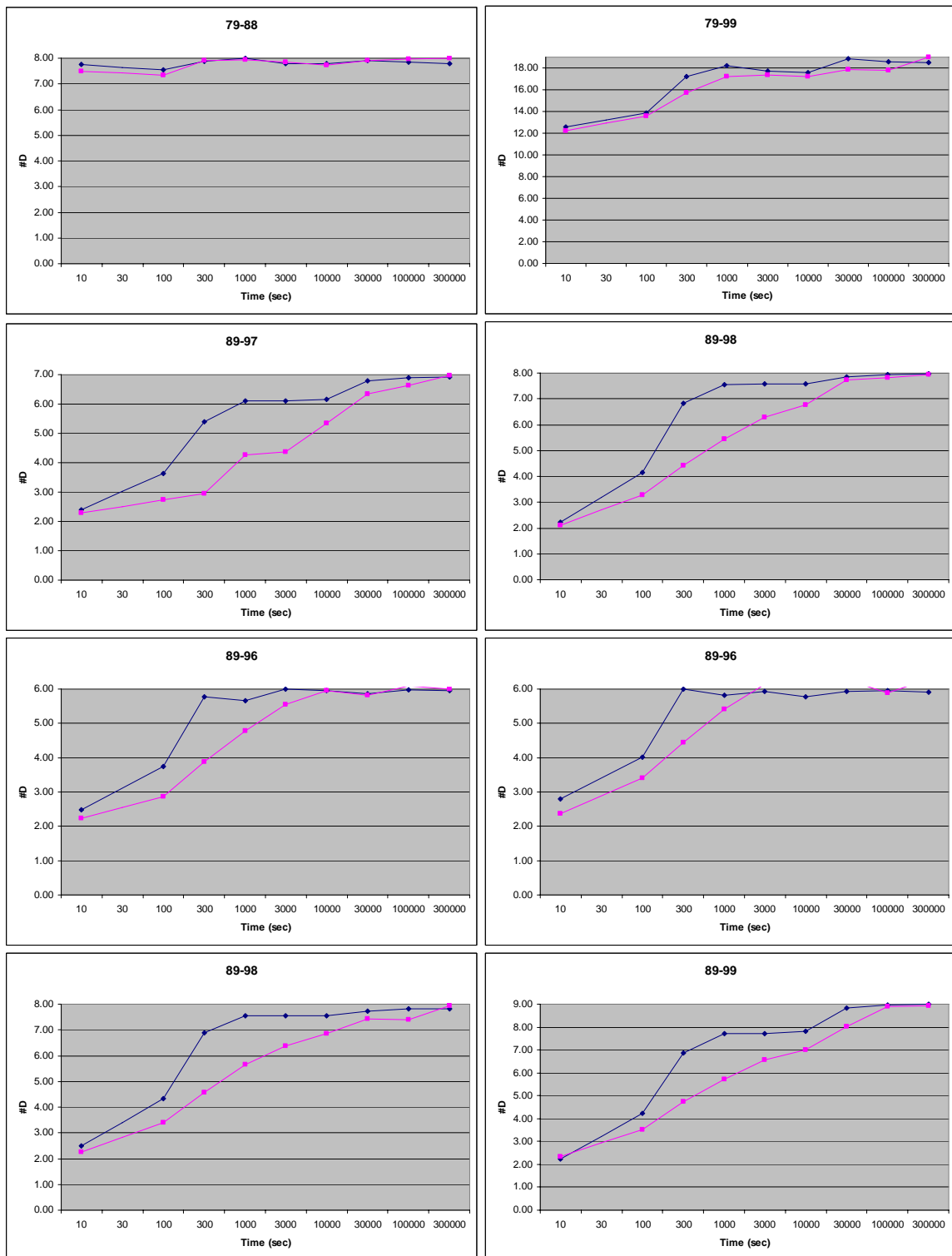


Table 1. Biochemical characteristics of eukaryotic glycogen, amylopectin, and Lafora bodies.

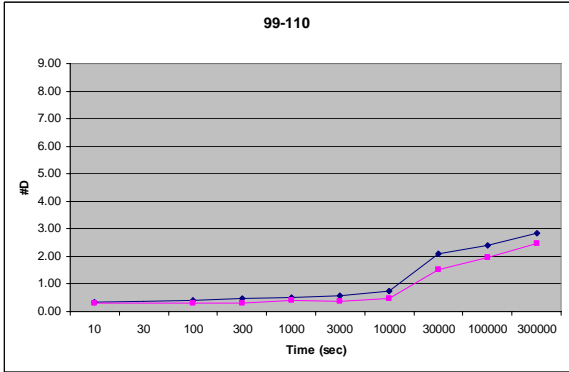
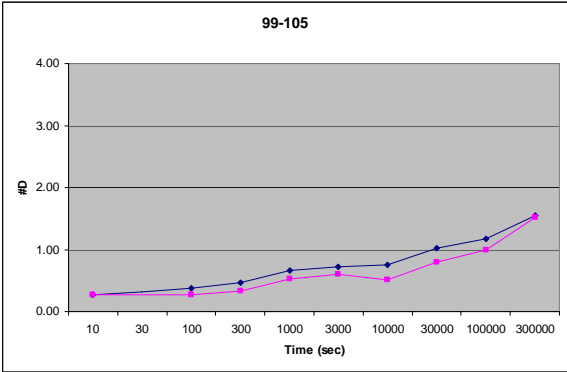
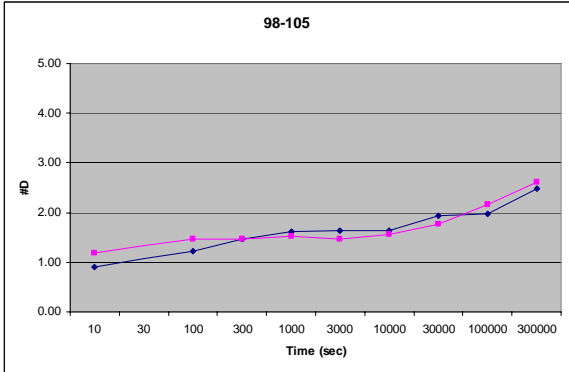
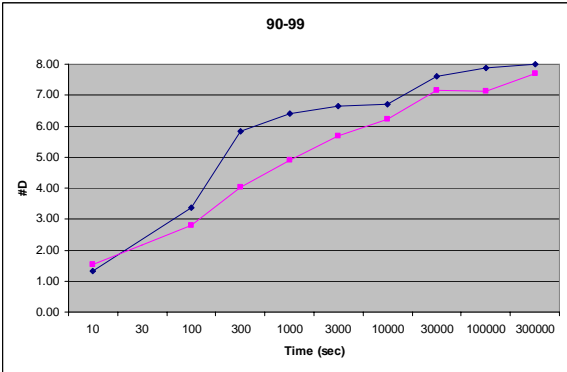
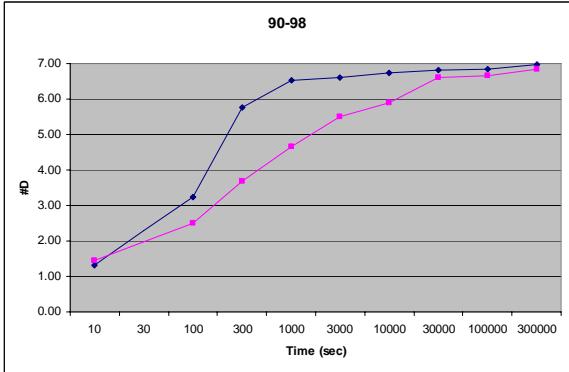
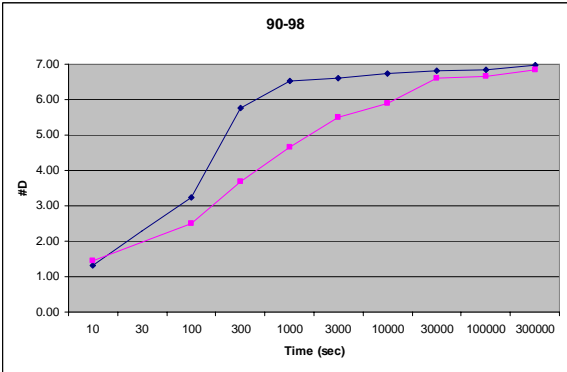
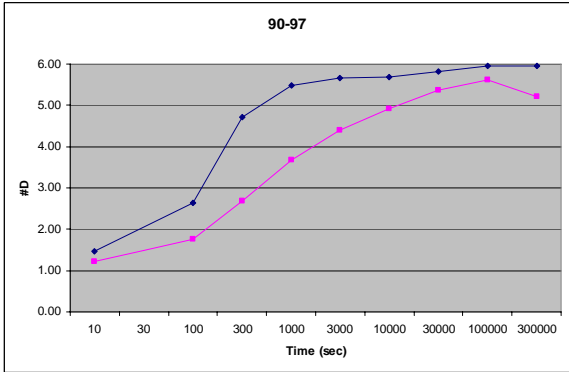
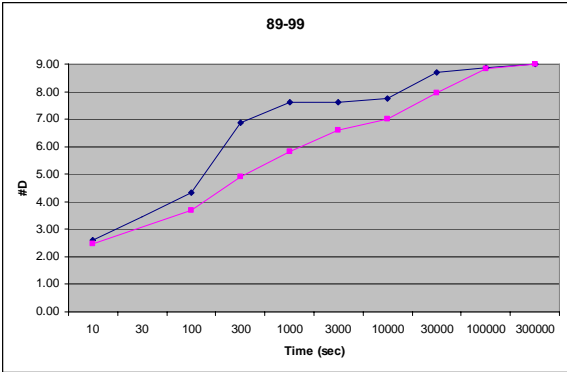
	<u>residues/ branch</u>	<u>branching pattern</u>	<u>water soluble</u>	<u>phosphate content</u>
Eukaryotic glycogen	12-14	continuous	yes	trace
Amylopectin	12-20	discontinuous	no	0.2-0.4% w/w
Lafora body	12-30+	discontinuous	no	> glycogen

Supplemental Figure 1. Number of deuterons incorporated in amylopectin-bound (purple) and apo- (blue) SEX4 as a function of time for all 156 peptides obtained. Subtract “2” from the first peptide number to obtain the corresponding residues that each peptide represents (assuming the first two amino acid residues back-exchange too rapidly to retain deuterons⁴⁵; this fact has been accounted for in our calculations for all graphs)

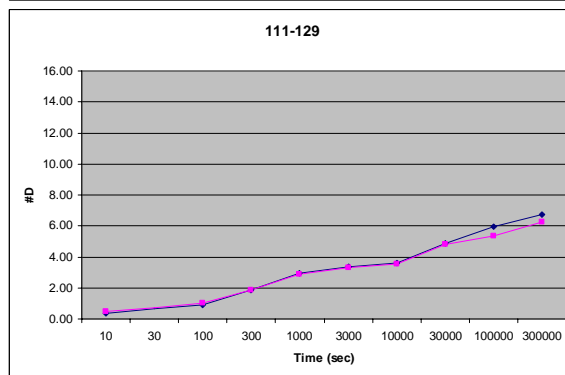
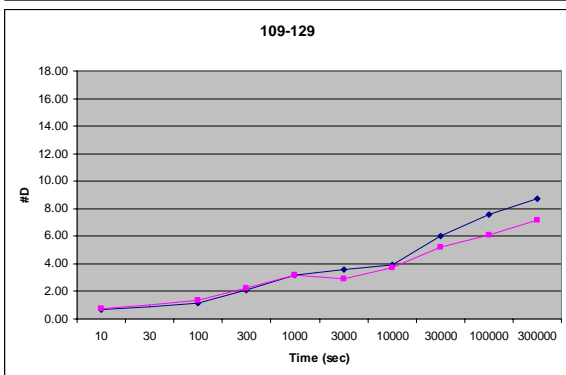
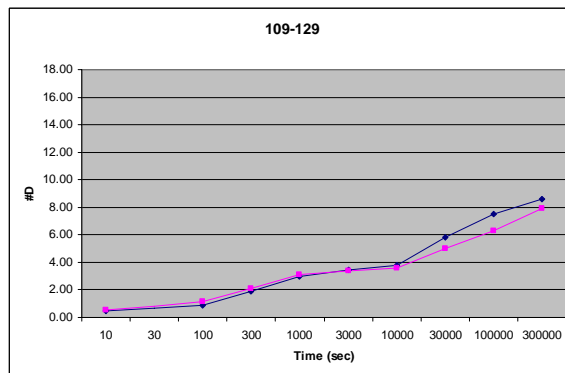
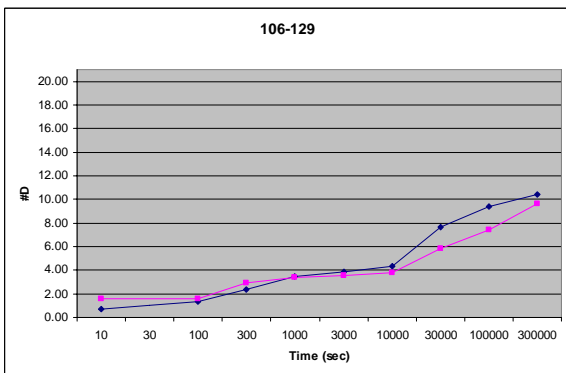
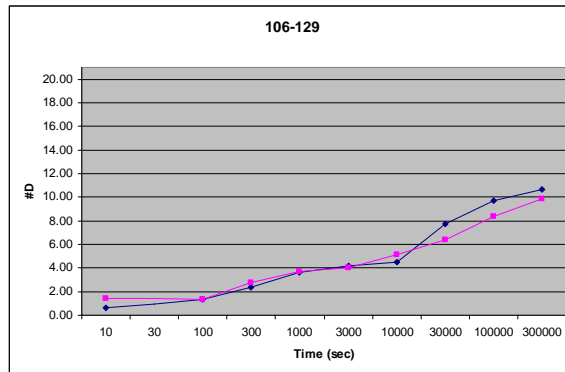
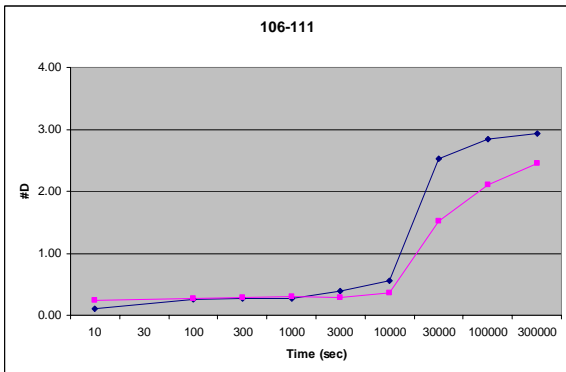
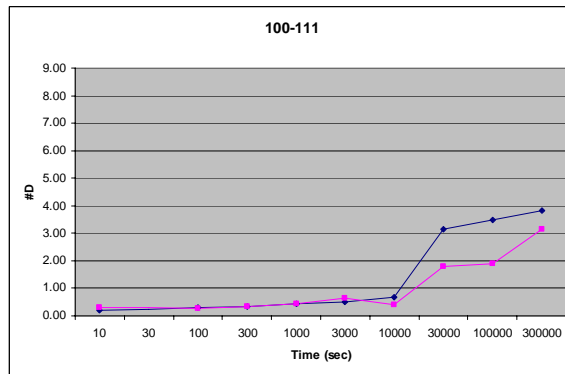
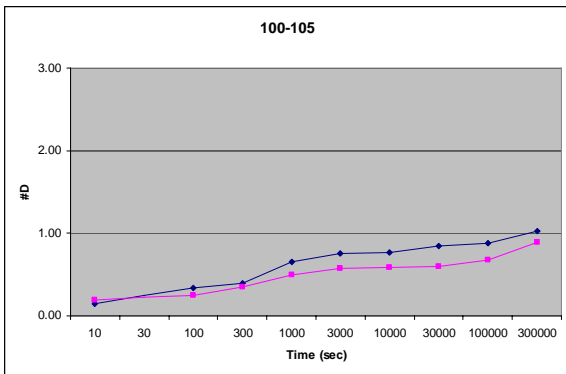
SUPPLEMENTAL FIGURES



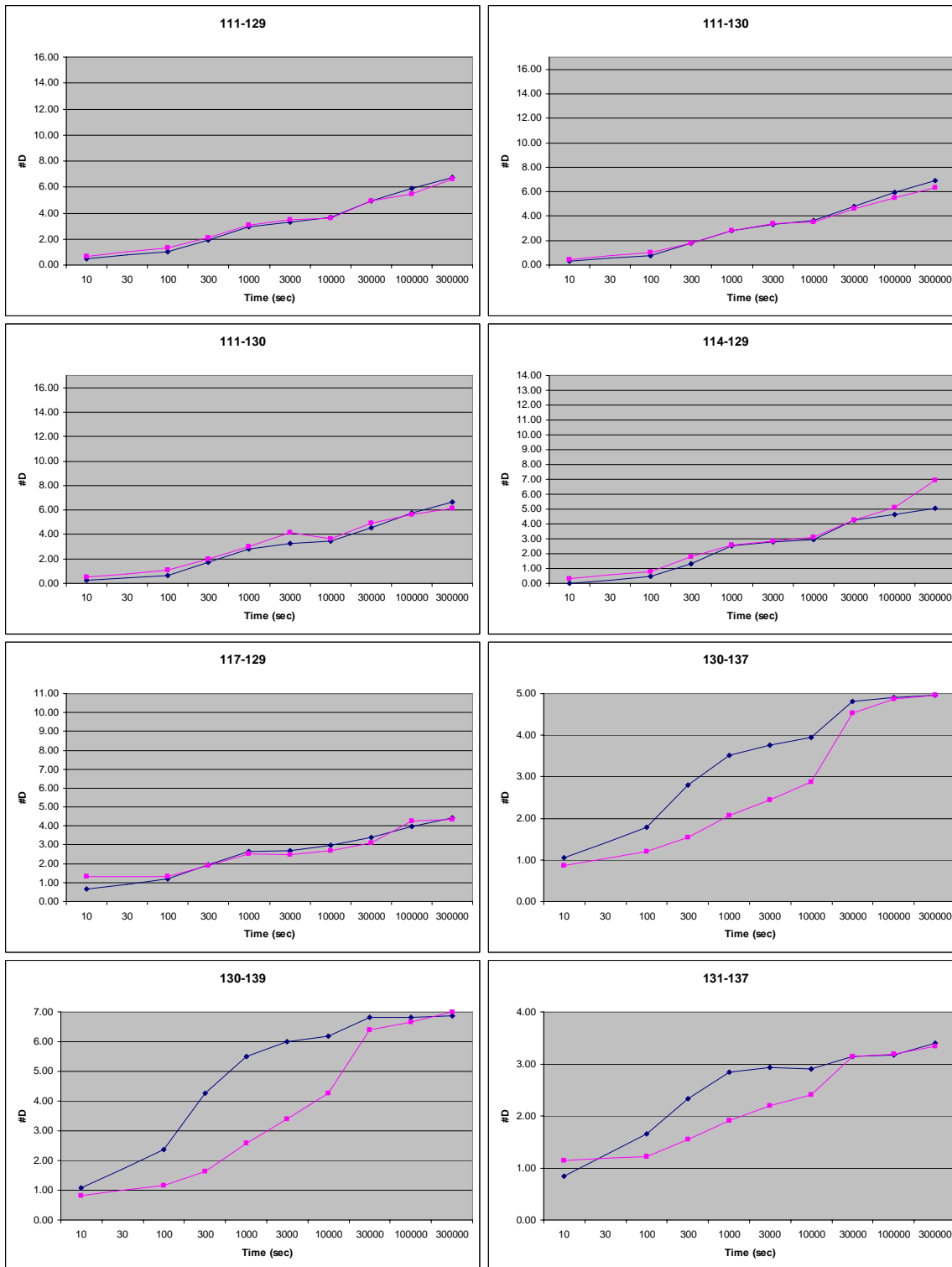
Supplemental Figure 1, Continued.



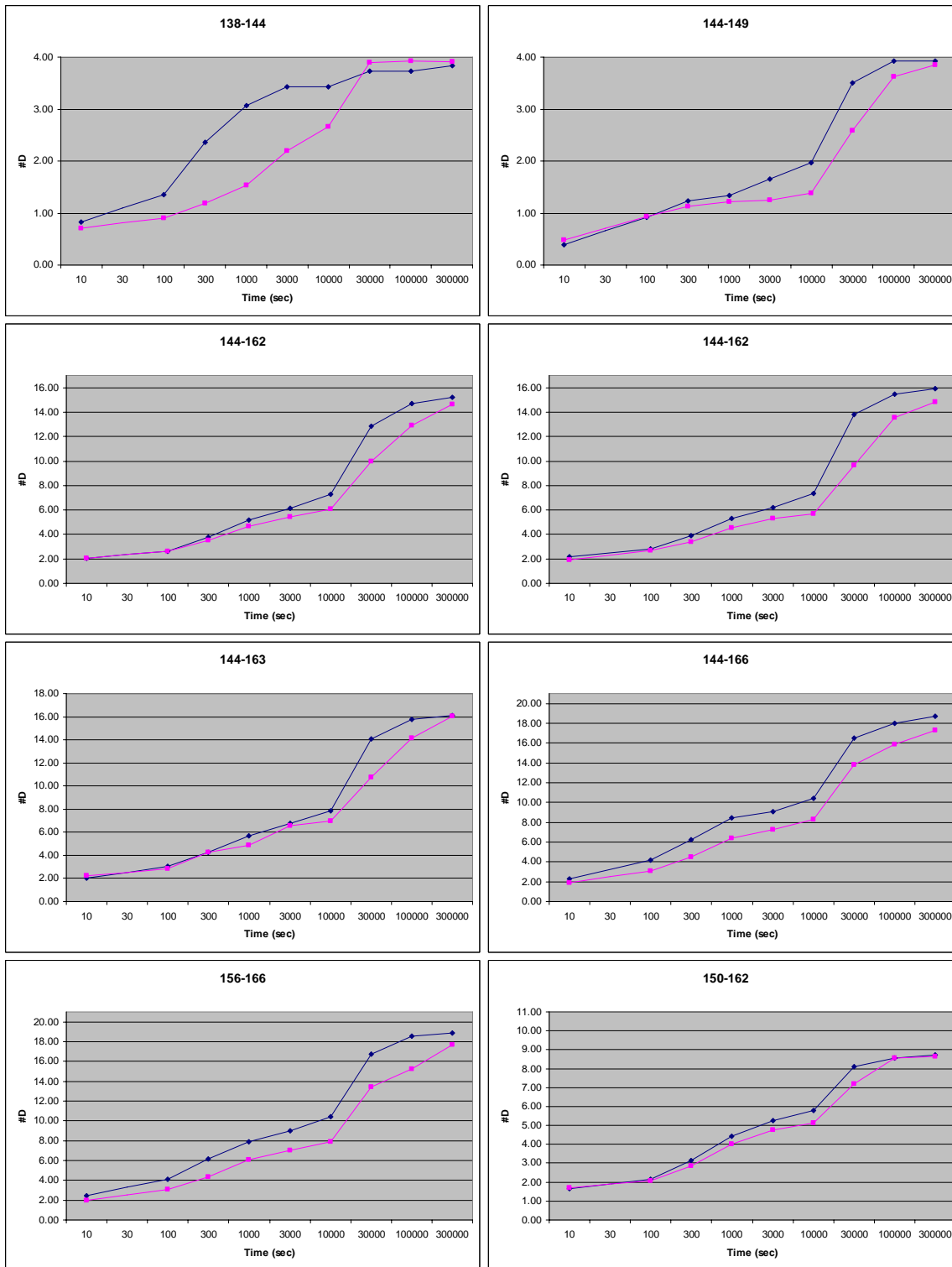
Supplemental Figure 1, Continued.



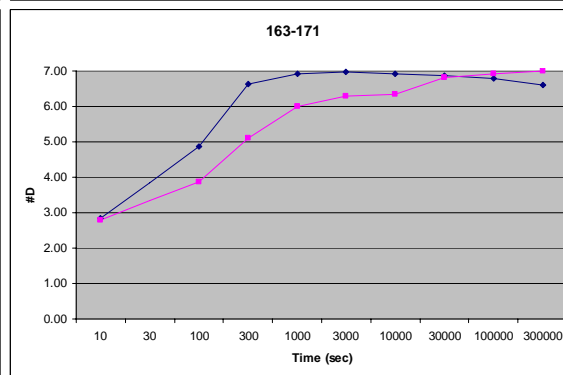
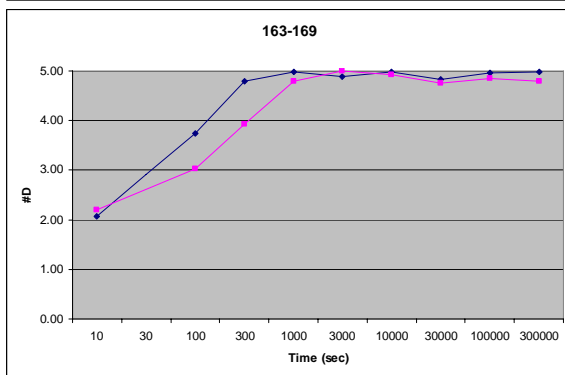
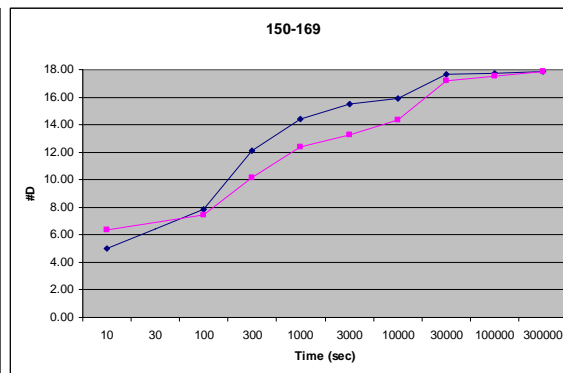
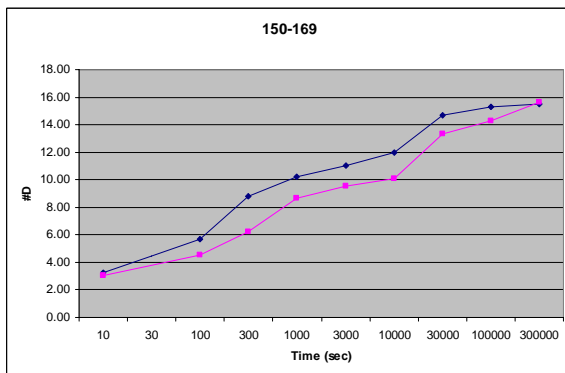
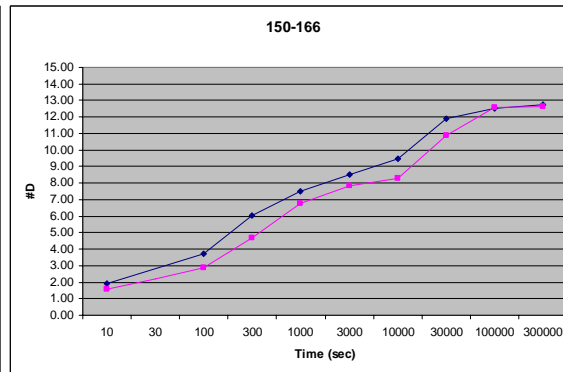
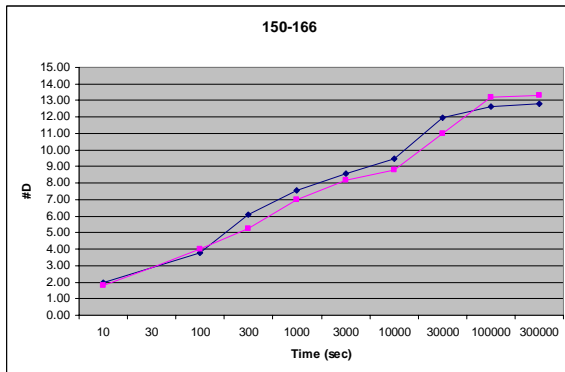
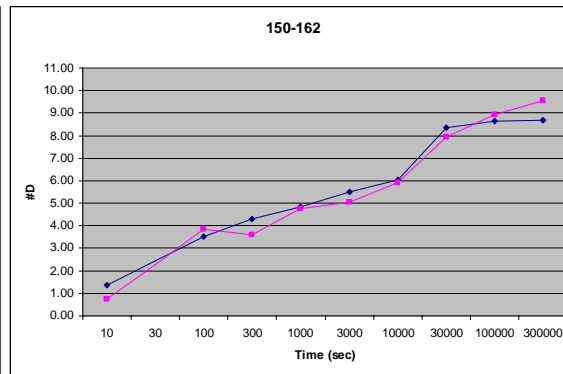
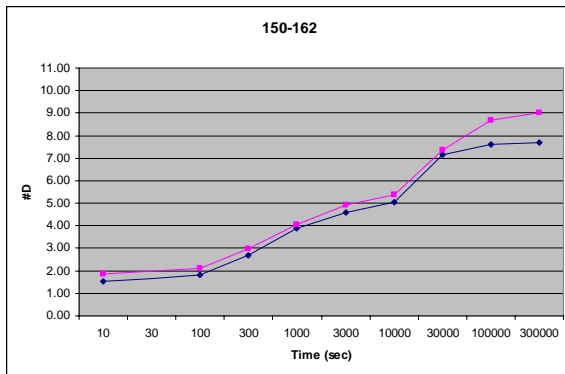
Supplemental Figure 1, Continued.



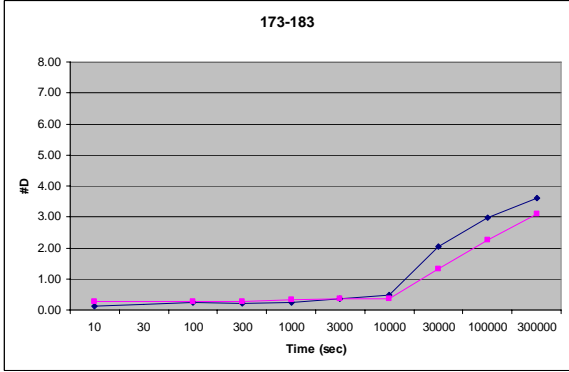
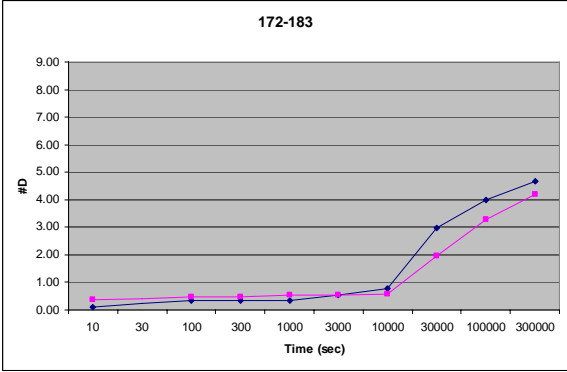
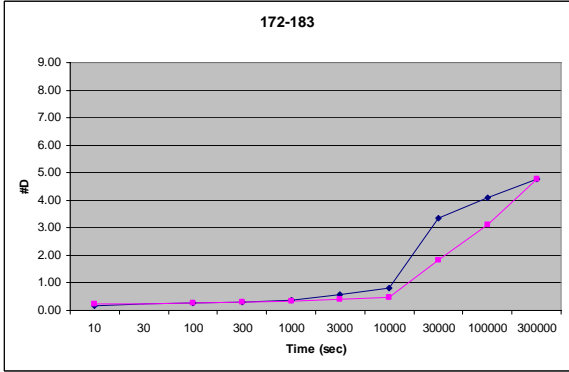
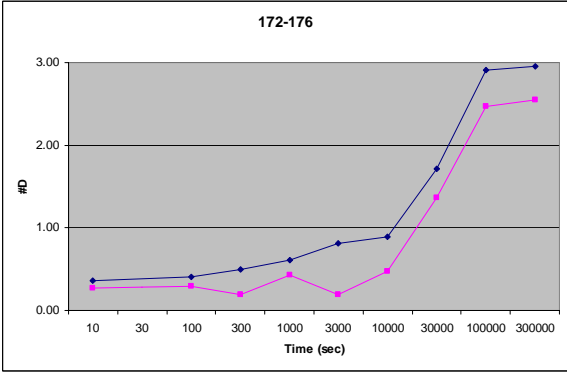
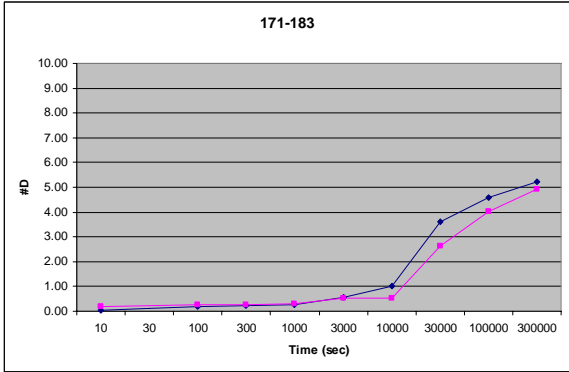
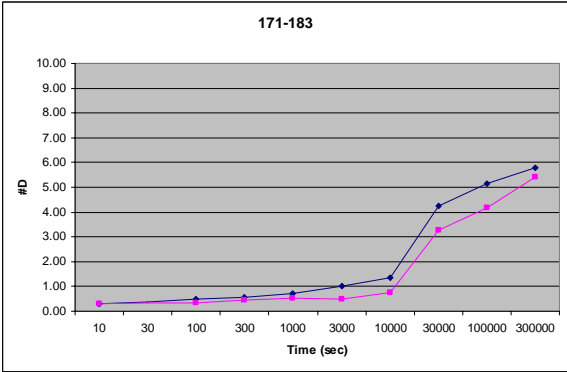
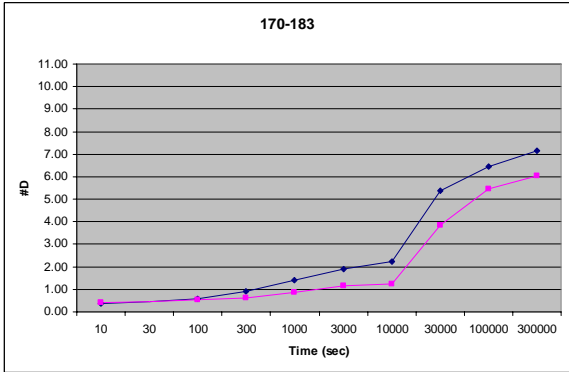
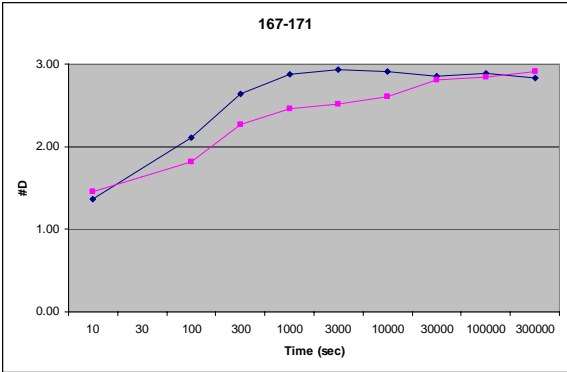
Supplemental Figure 1, Continued.



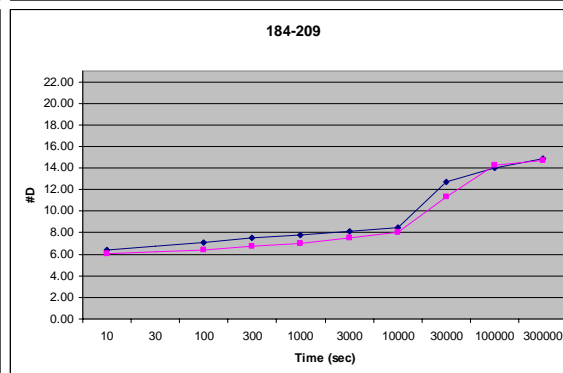
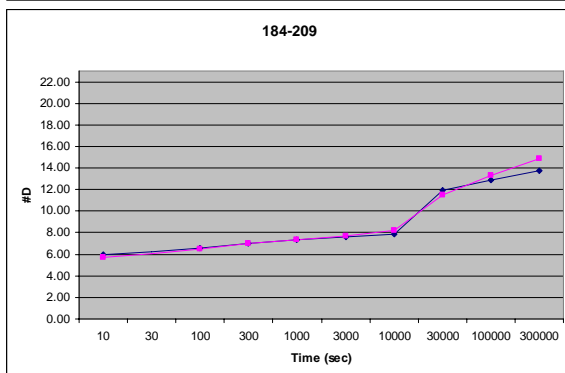
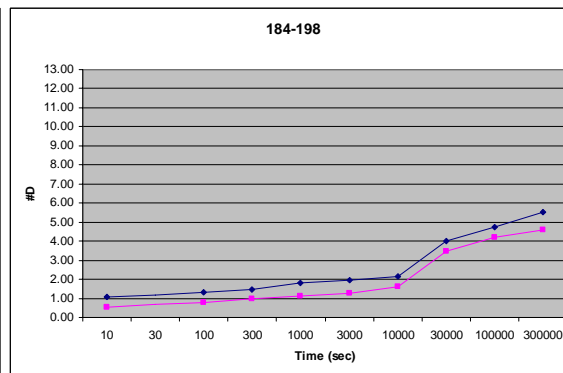
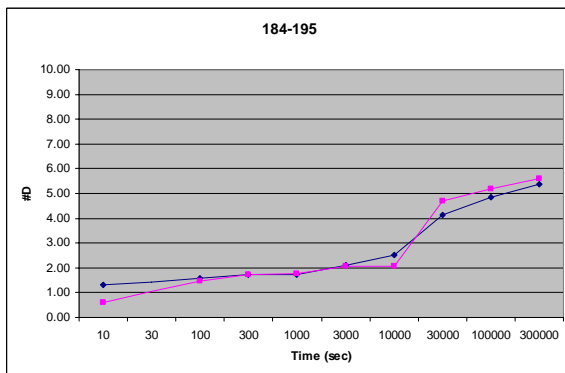
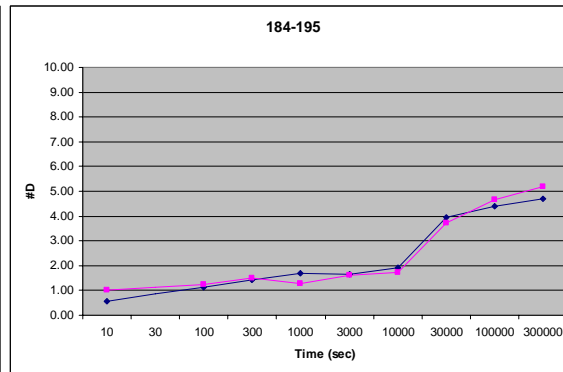
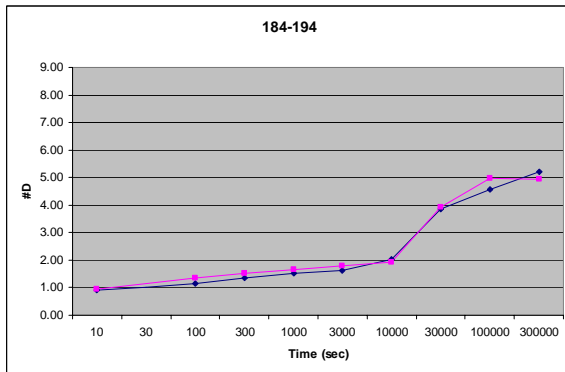
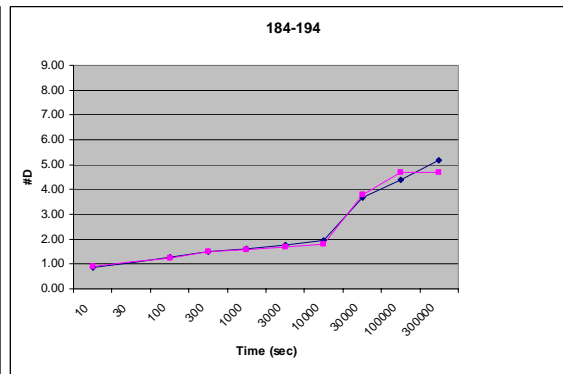
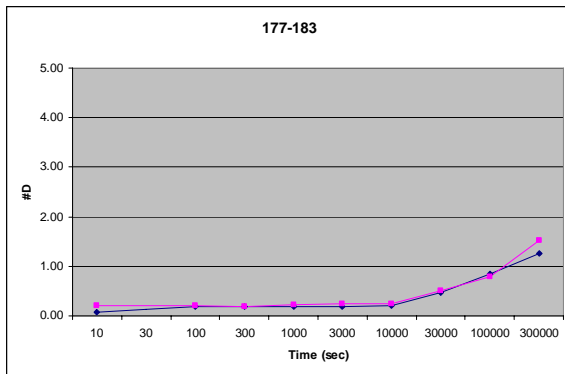
Supplemental Figure 1, Continued.



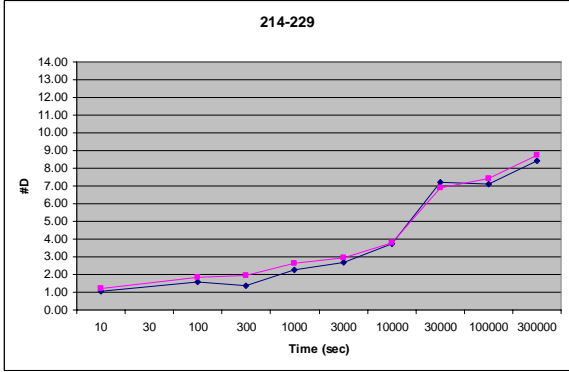
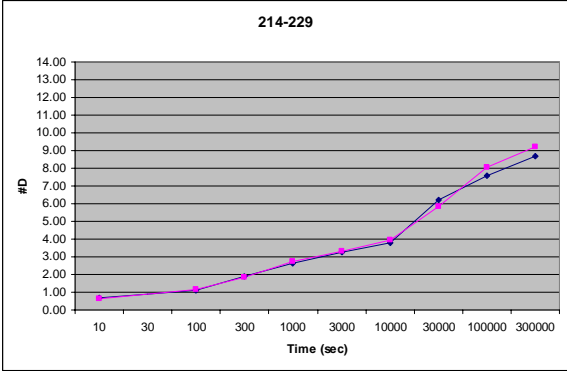
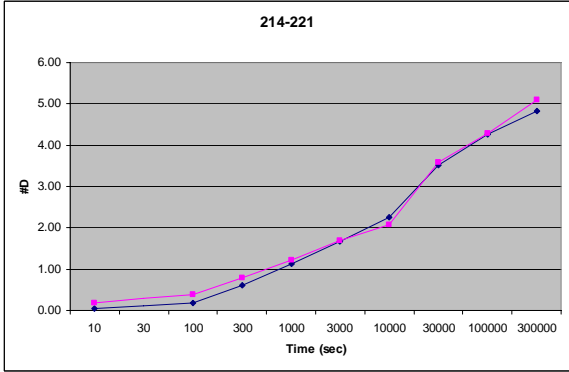
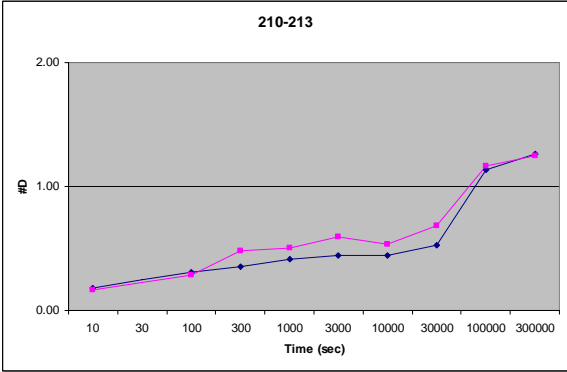
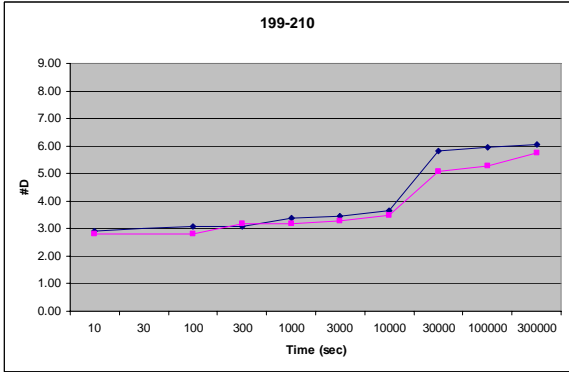
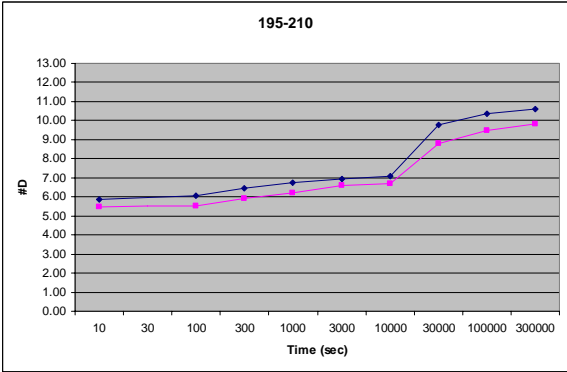
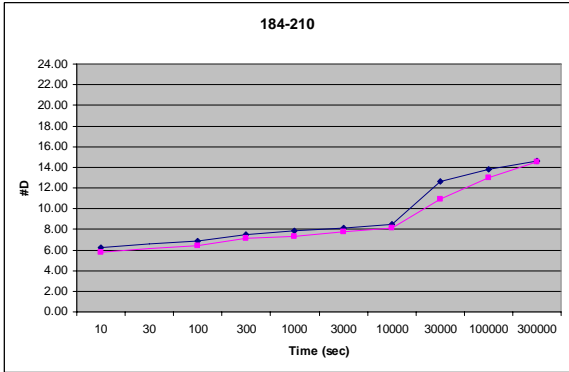
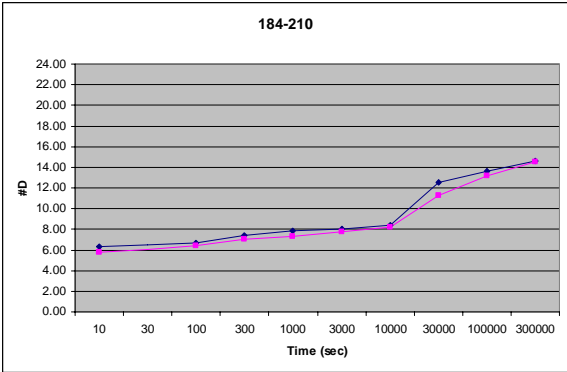
Supplemental Figure 1, Continued.



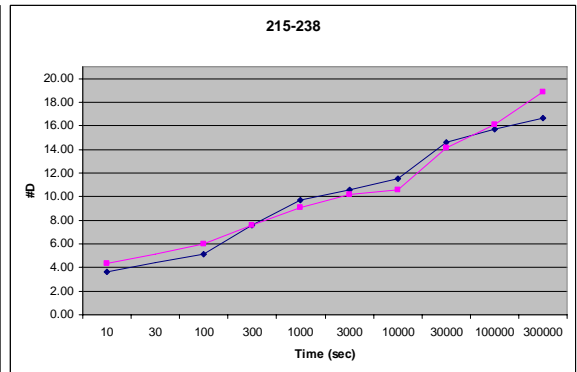
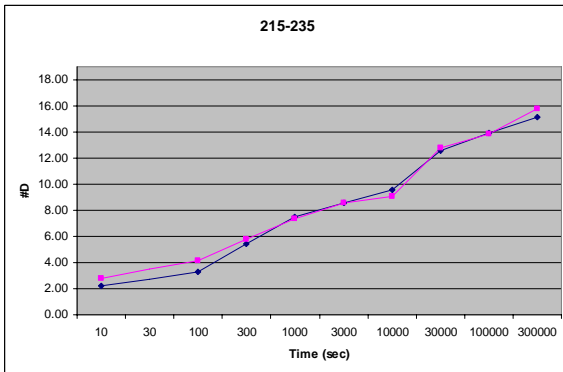
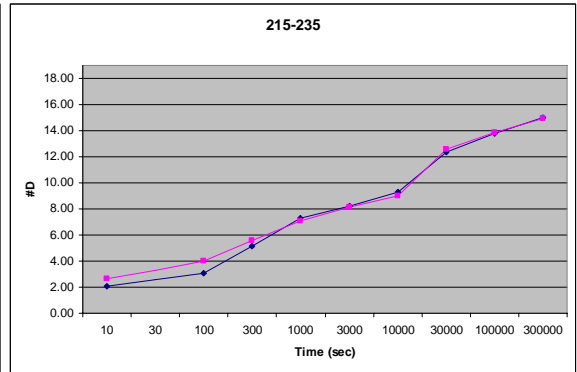
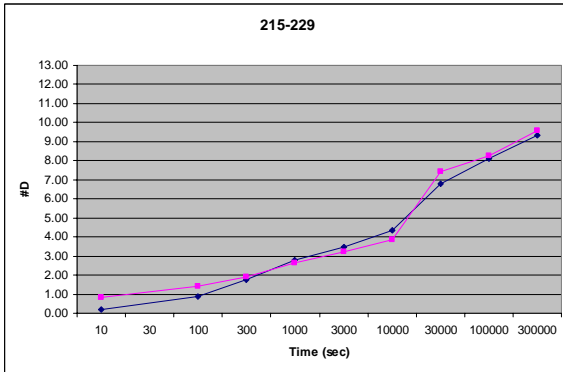
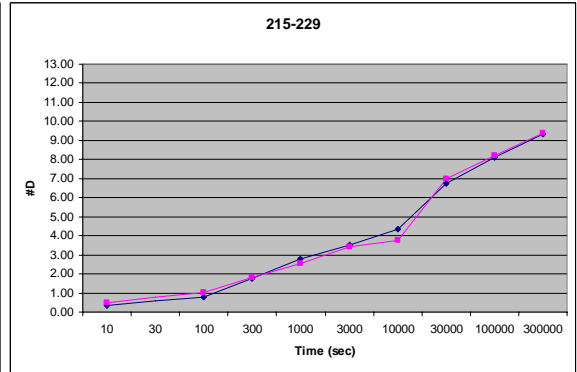
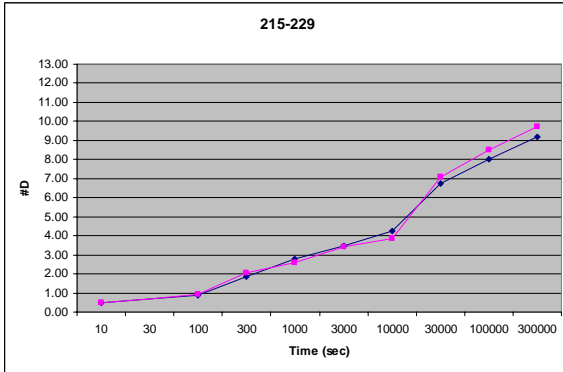
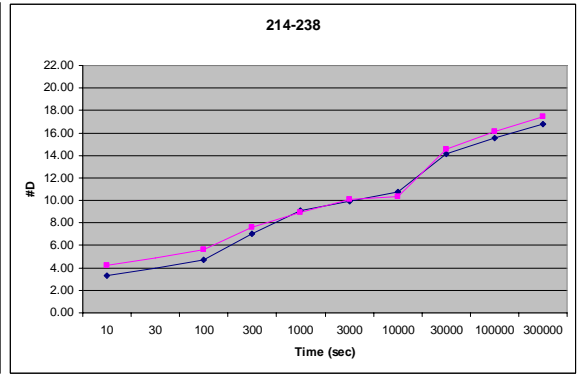
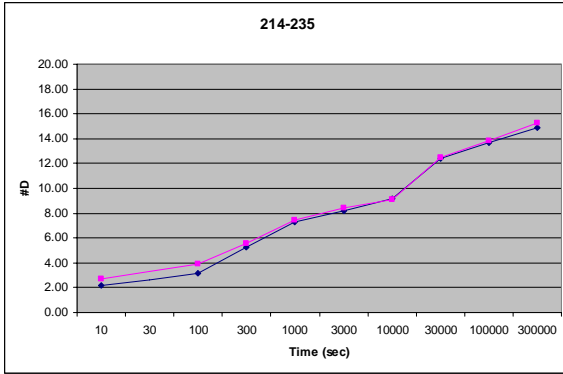
Supplemental Figure 1, Continued.



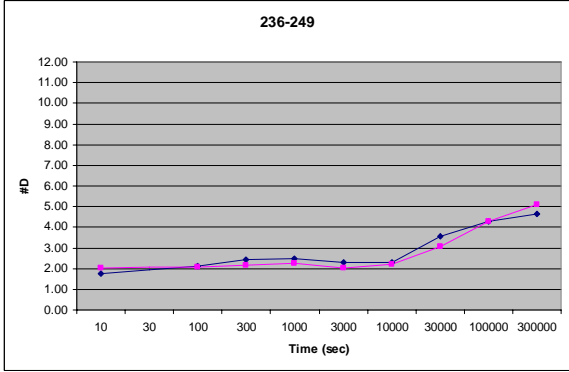
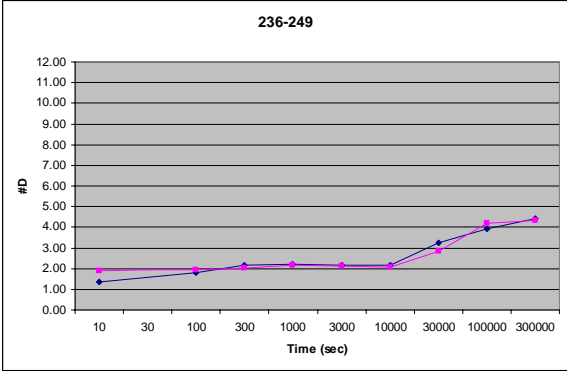
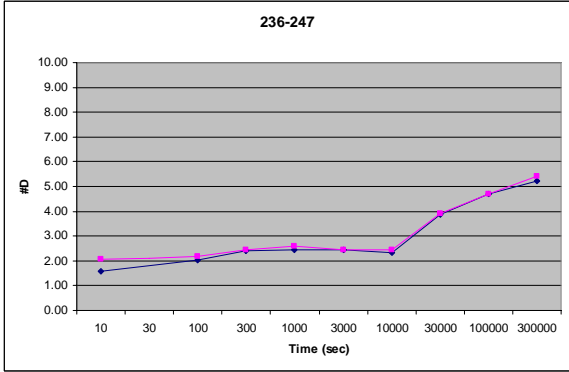
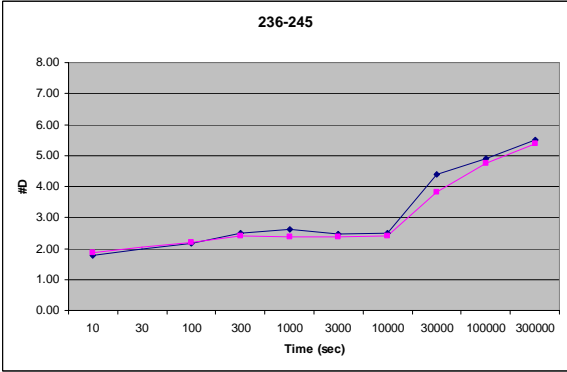
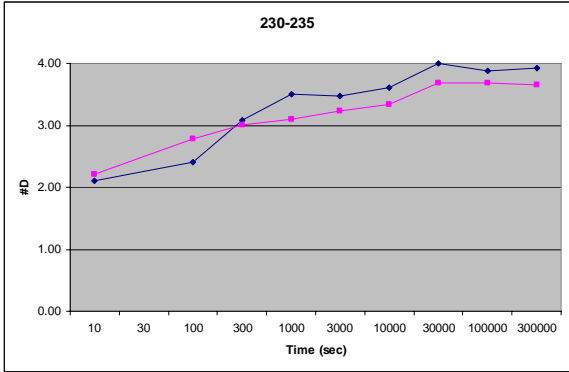
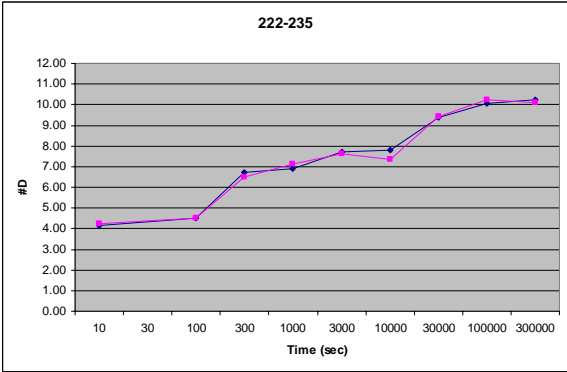
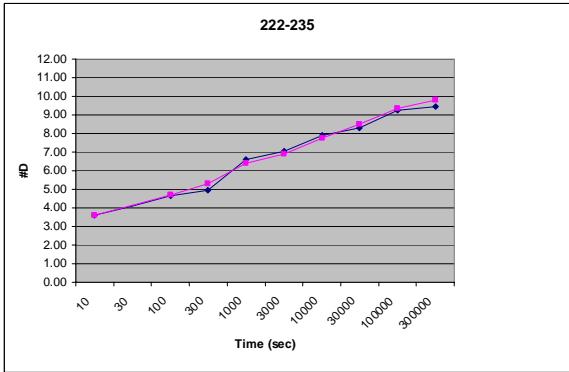
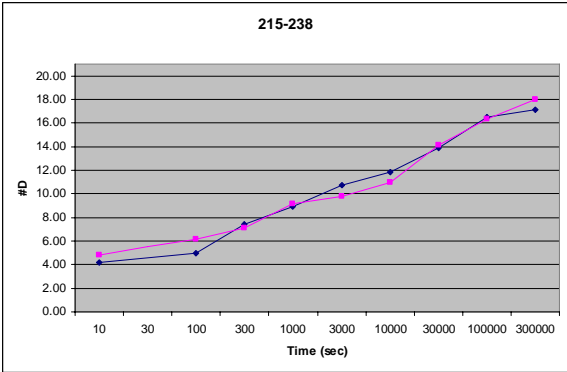
Supplemental Figure 1, Continued.



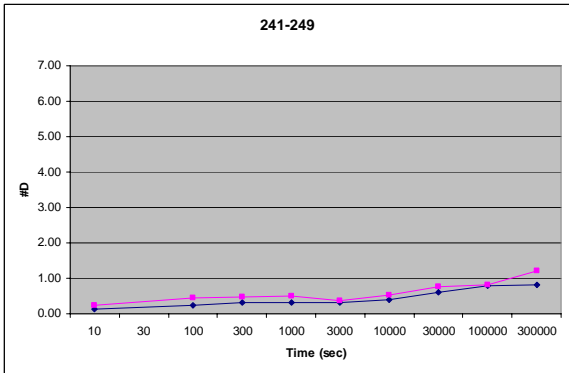
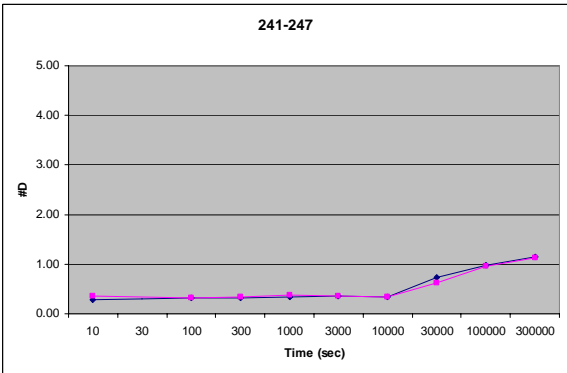
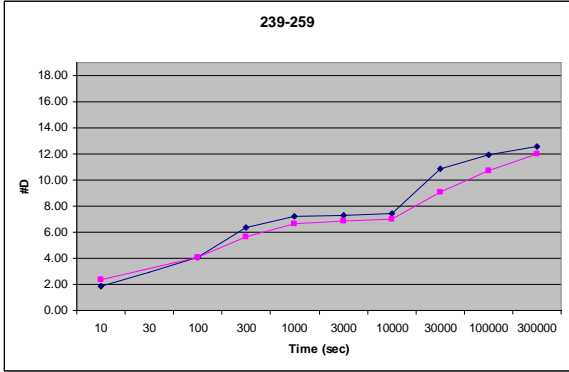
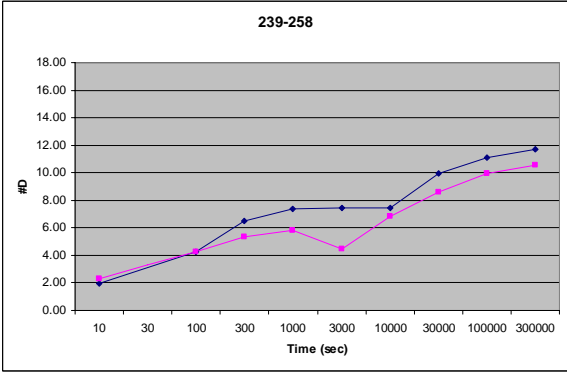
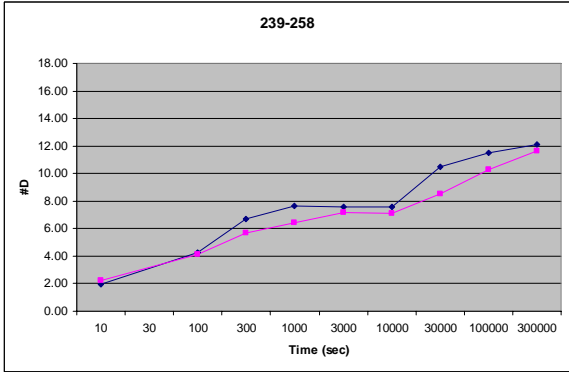
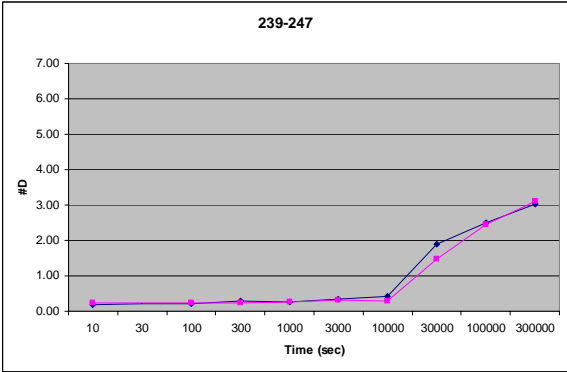
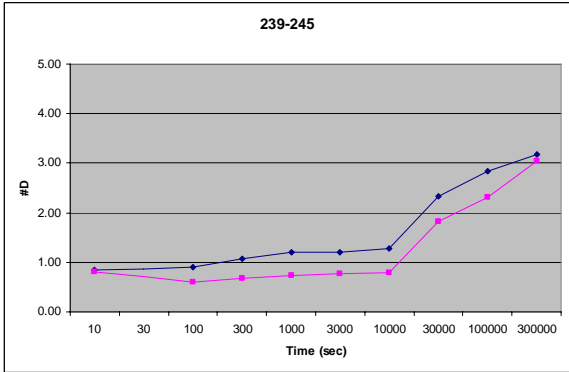
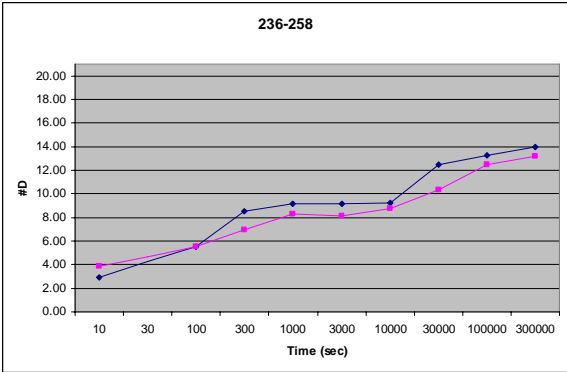
Supplemental Figure 1, Continued.



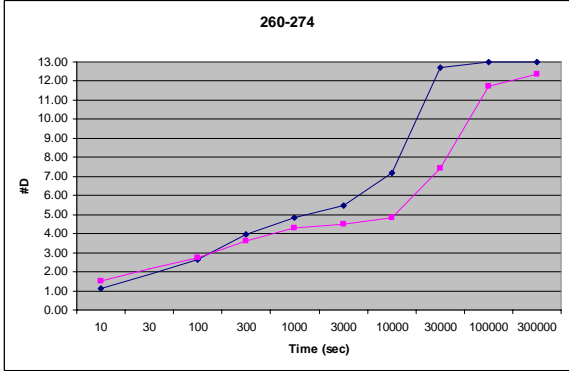
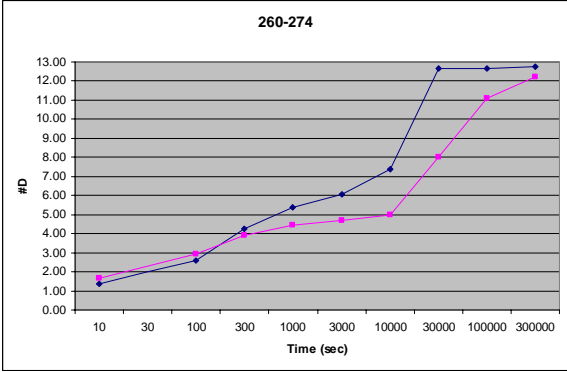
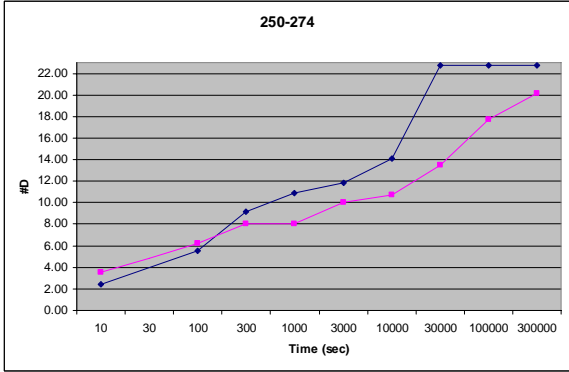
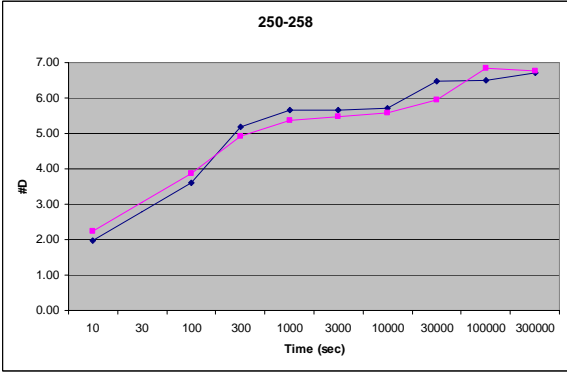
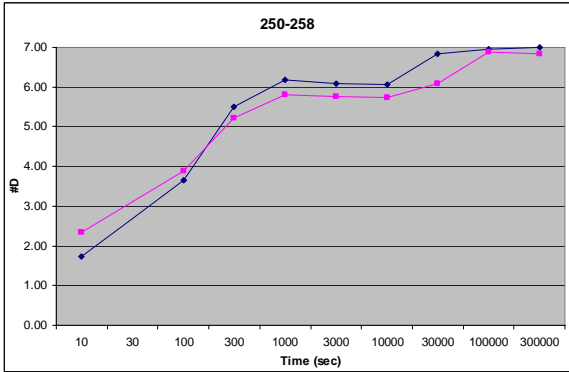
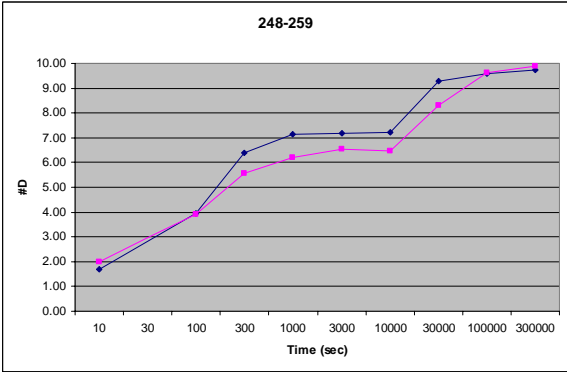
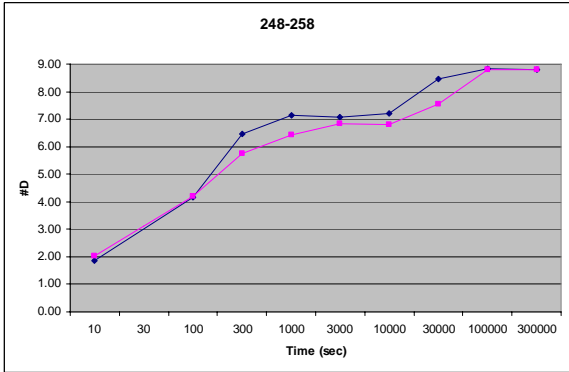
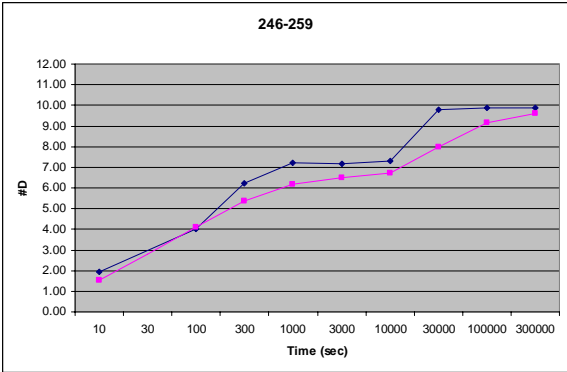
Supplemental Figure 1, Continued.



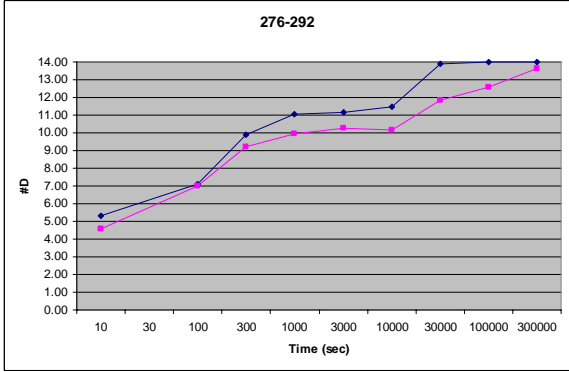
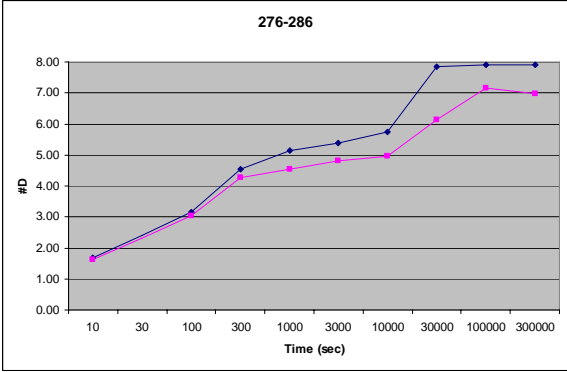
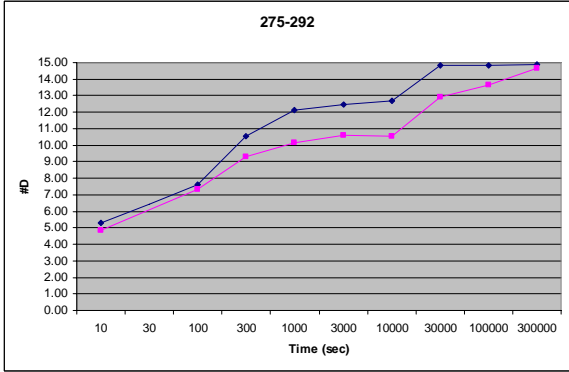
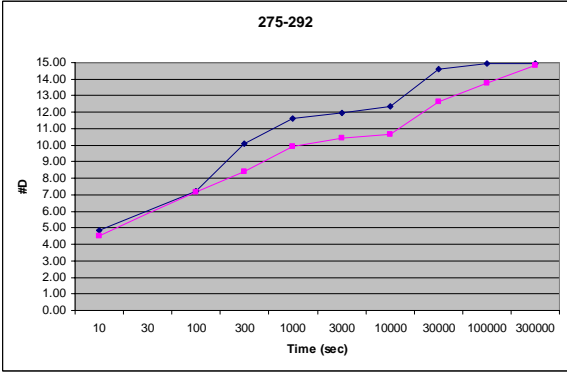
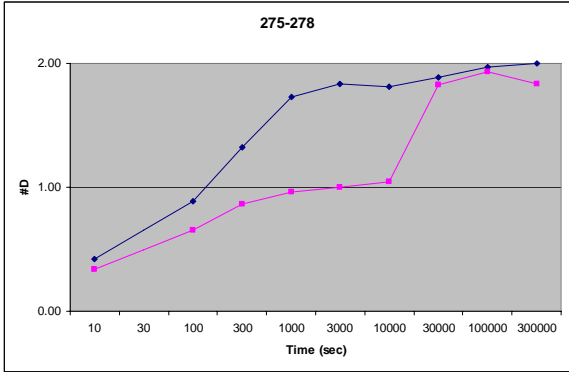
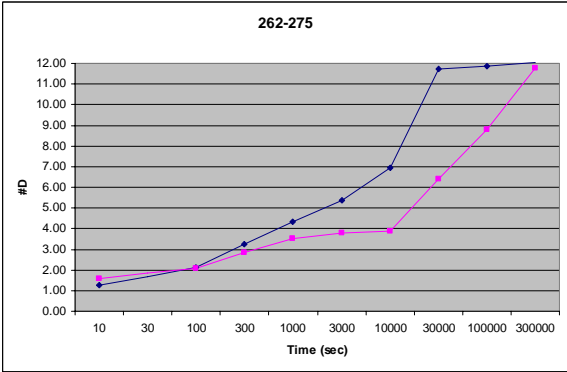
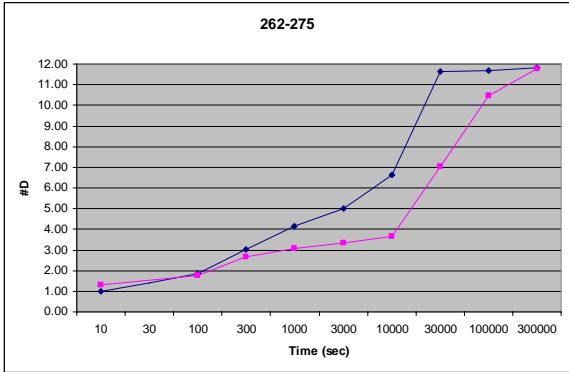
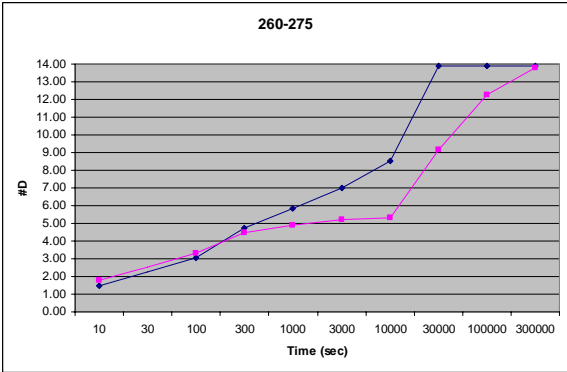
Supplemental Figure 1, Continued.



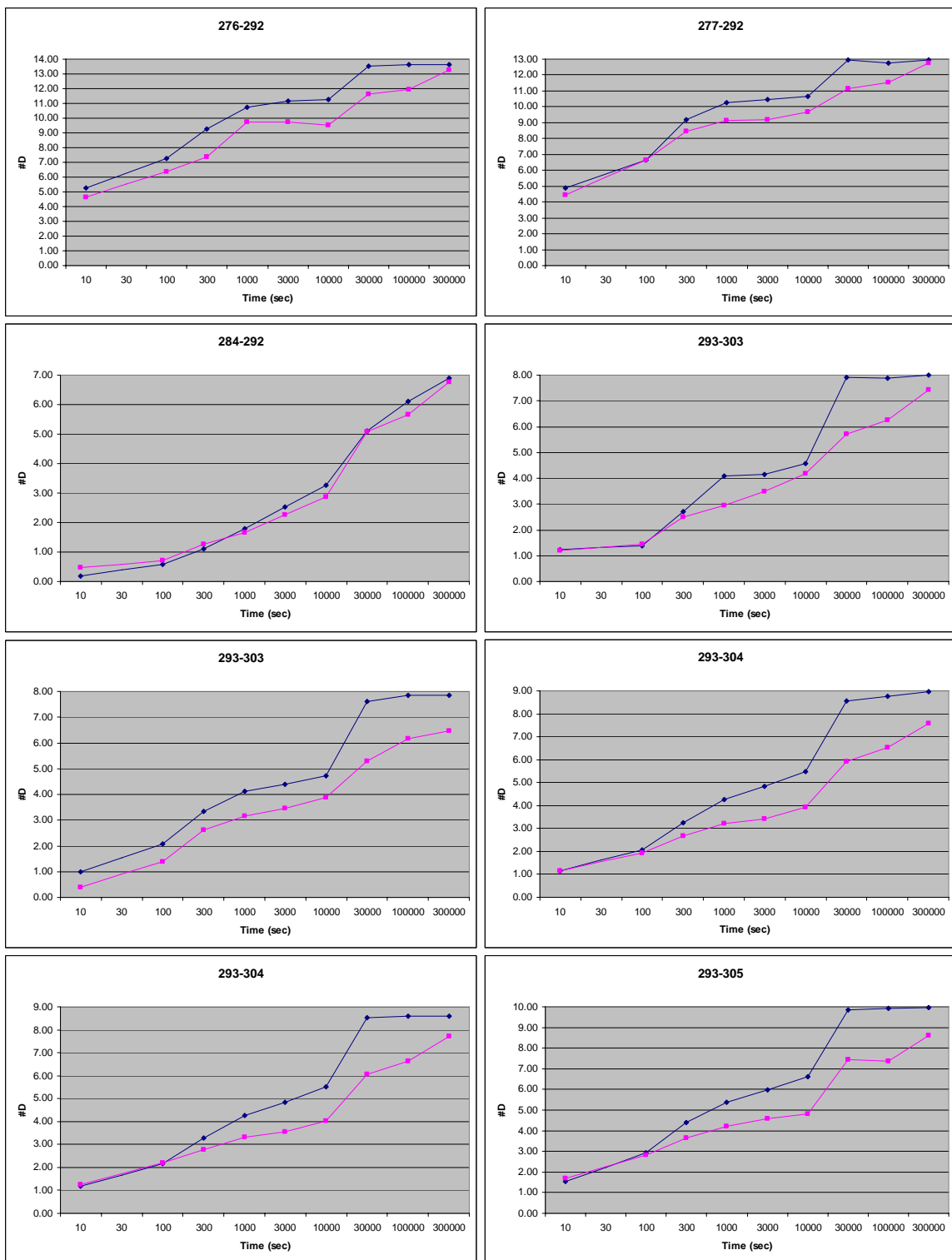
Supplemental Figure 1, Continued.



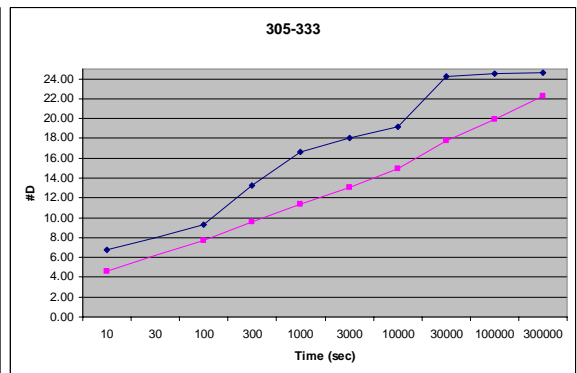
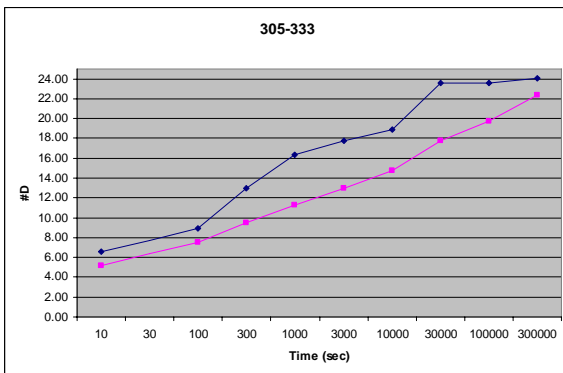
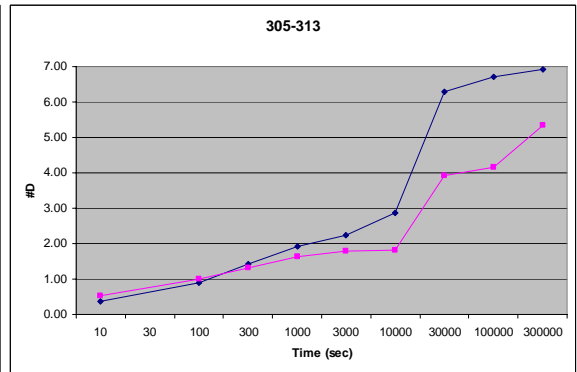
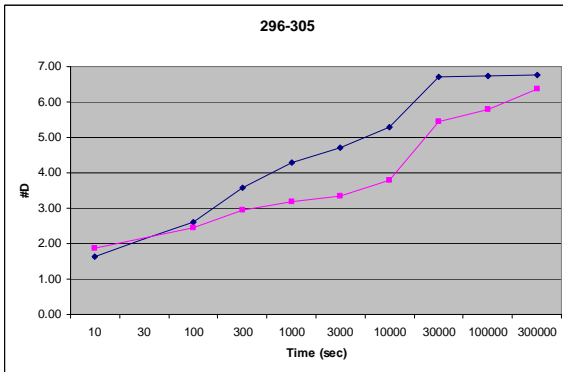
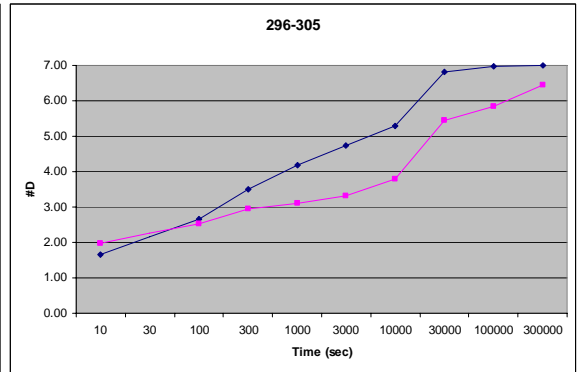
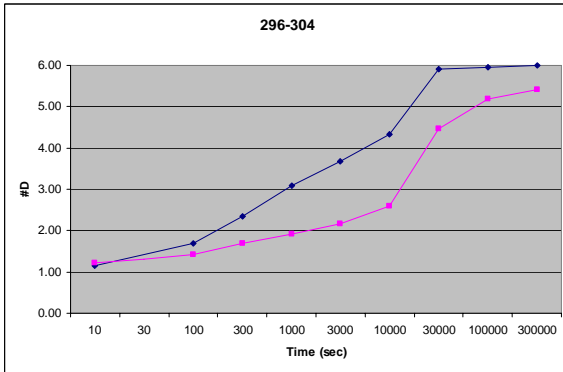
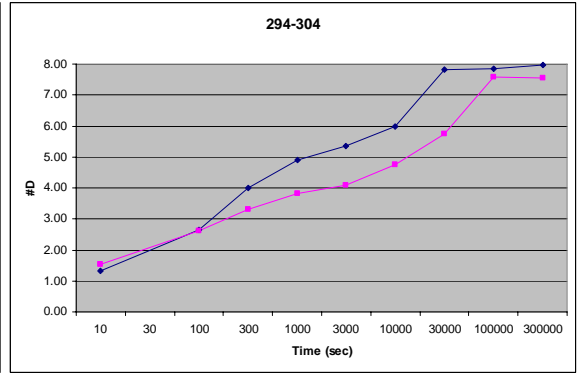
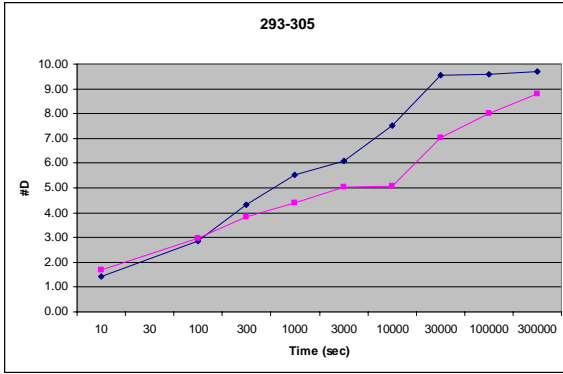
Supplemental Figure 1, Continued.



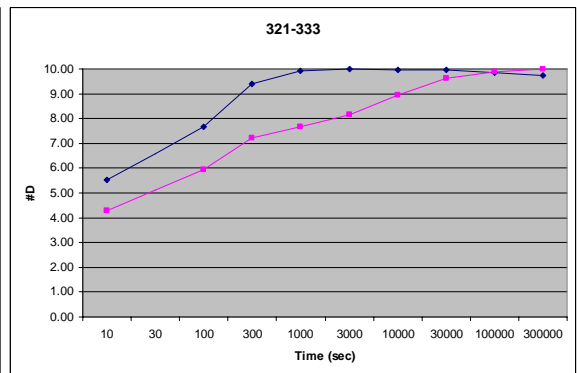
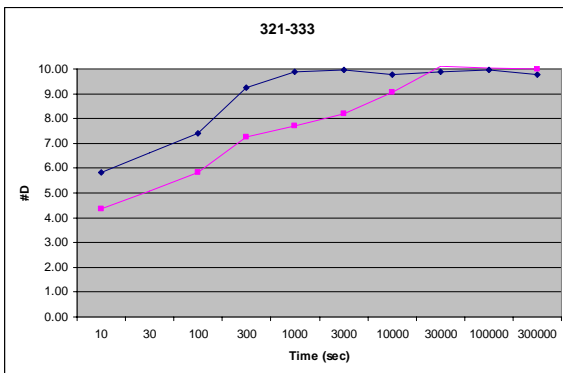
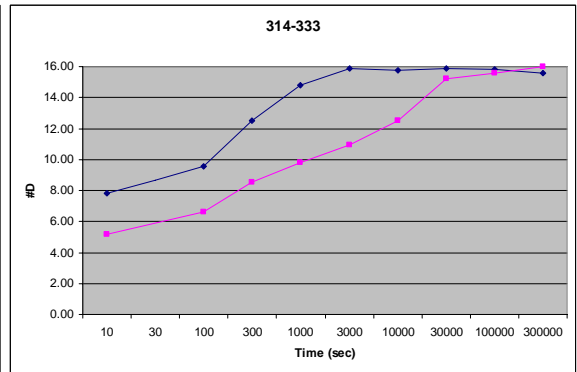
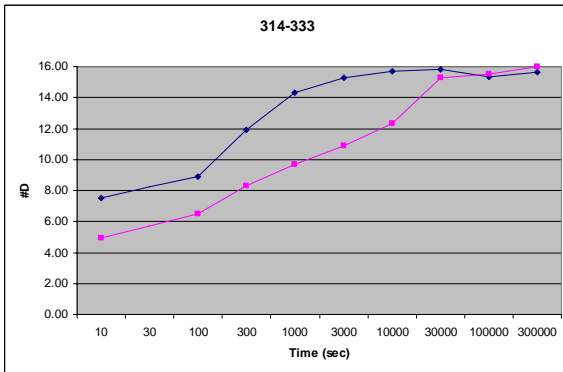
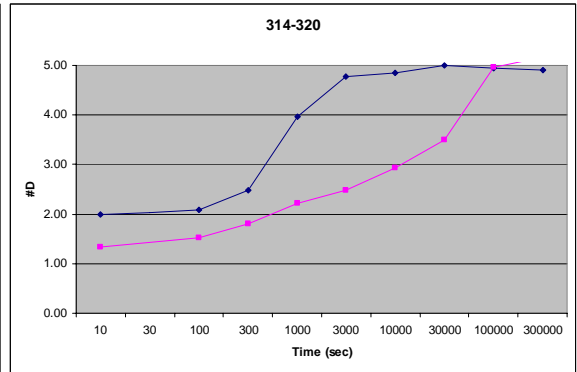
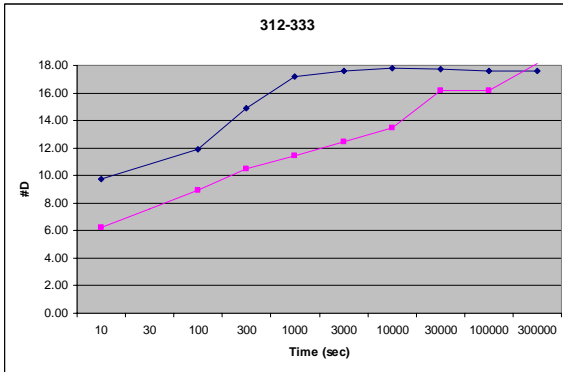
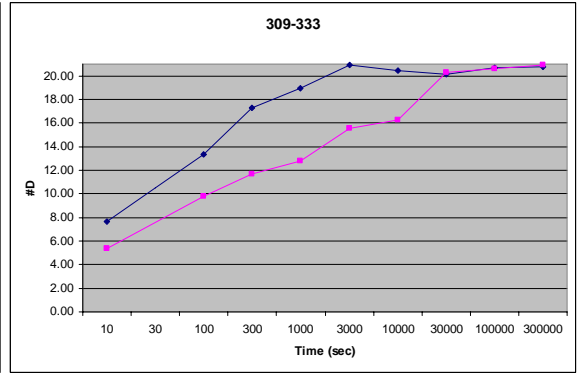
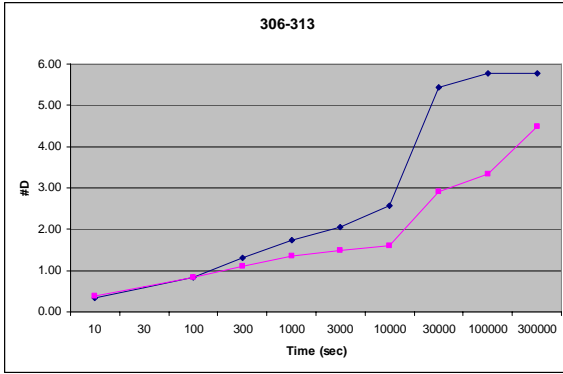
Supplemental Figure 1, Continued.



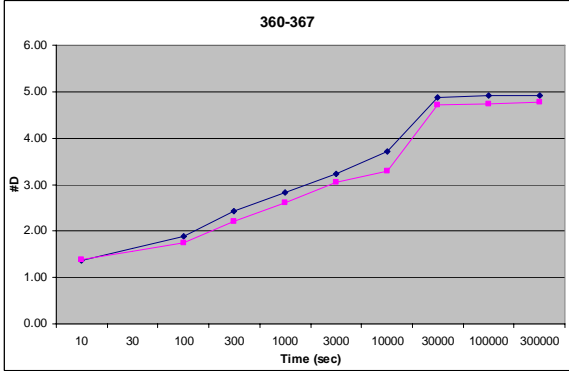
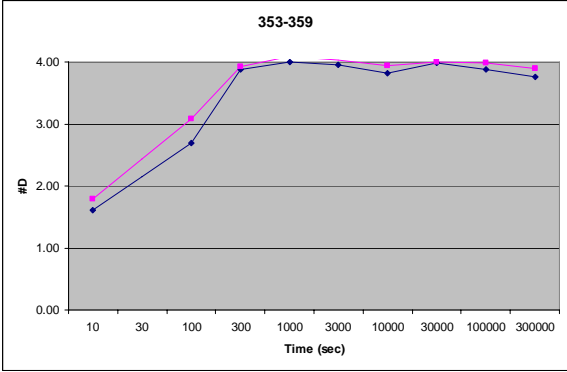
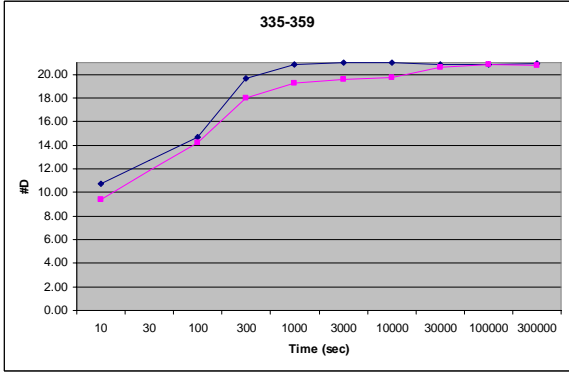
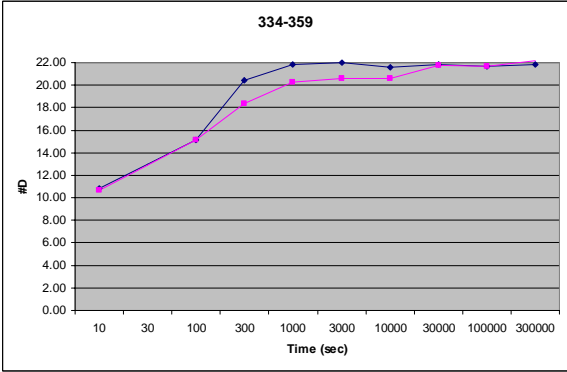
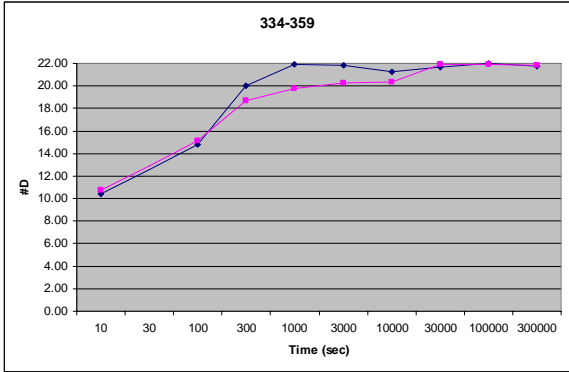
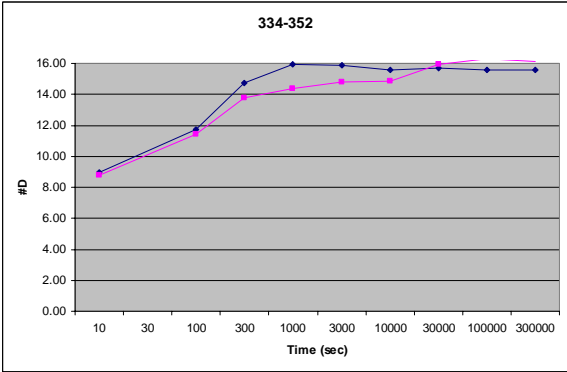
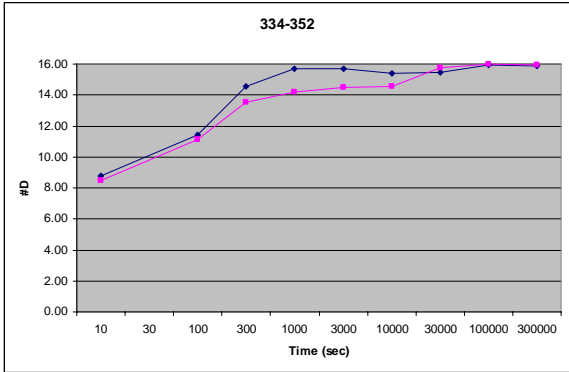
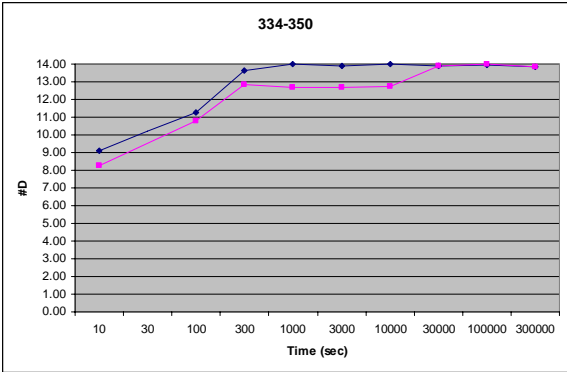
Supplemental Figure 1, Continued.



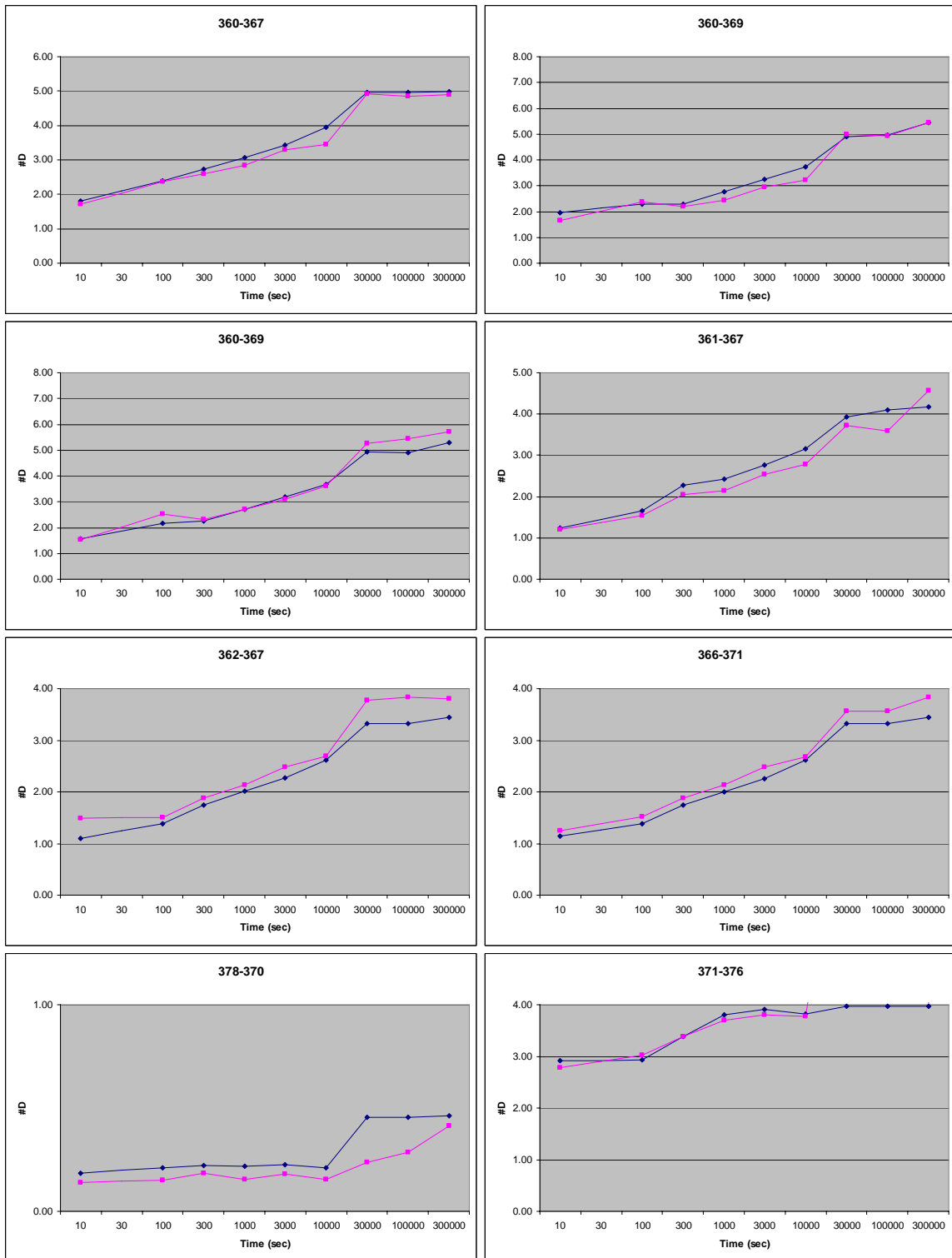
Supplemental Figure 1, Continued.



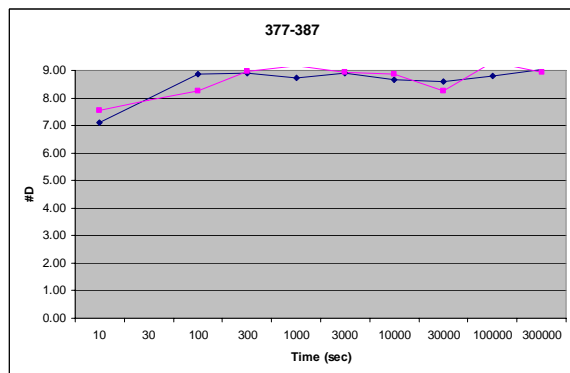
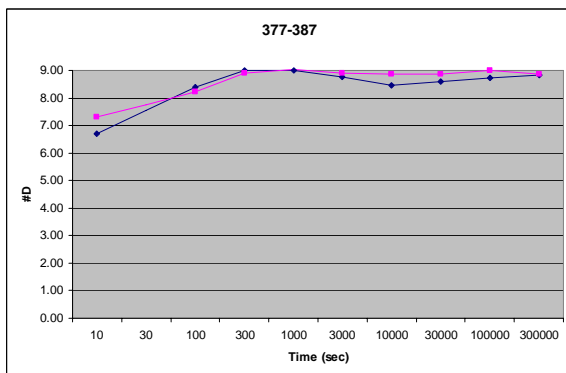
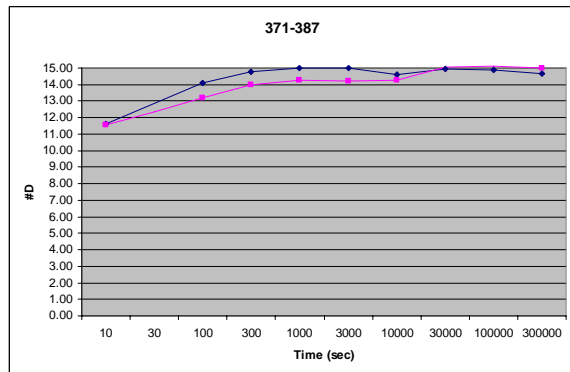
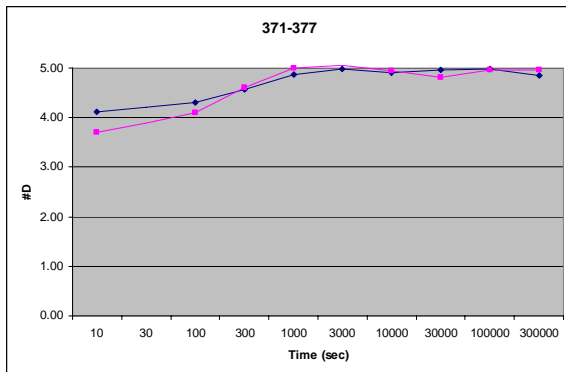
Supplemental Figure 1, Continued.



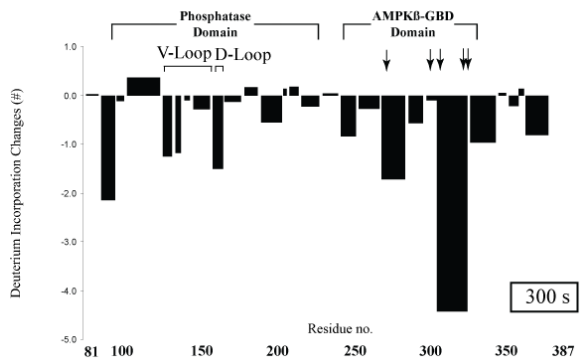
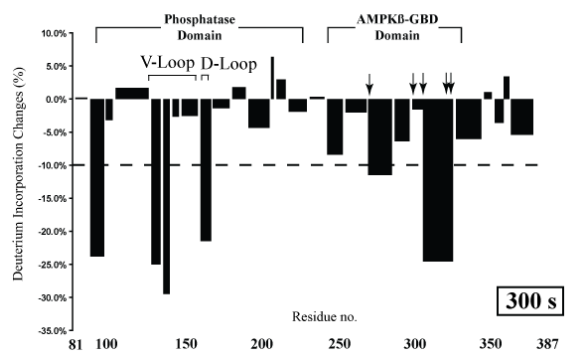
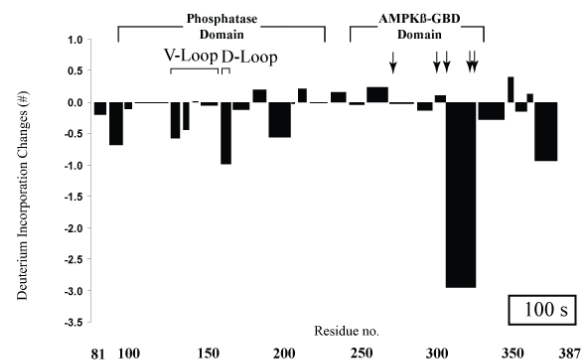
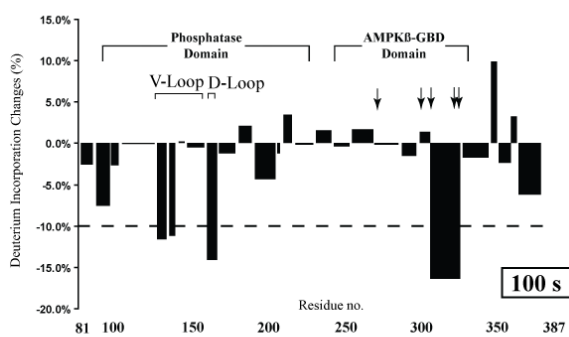
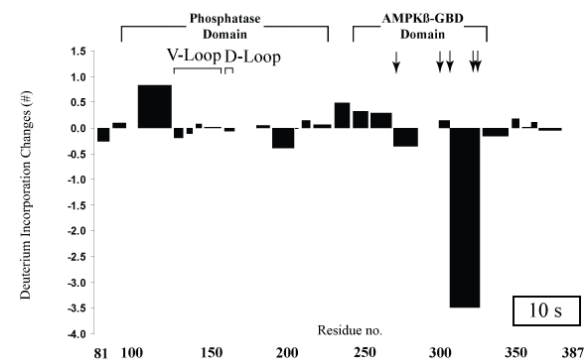
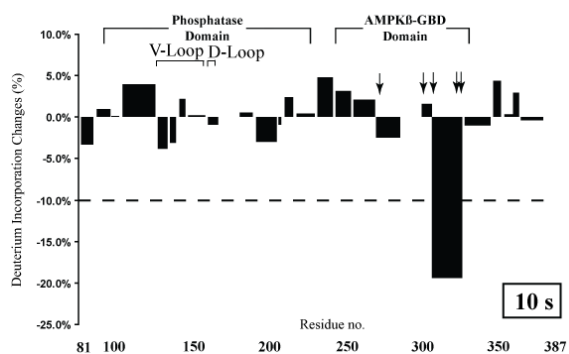
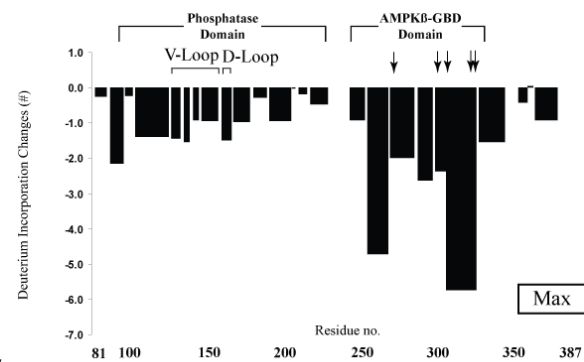
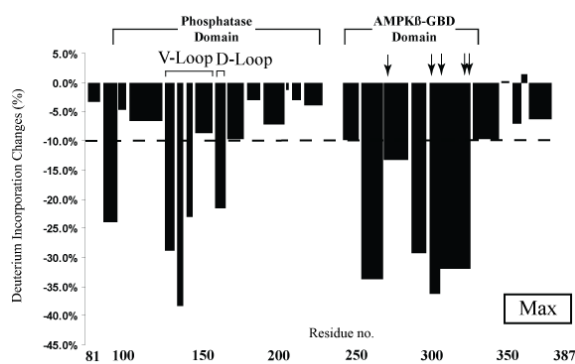
Supplemental Figure 1, Continued.



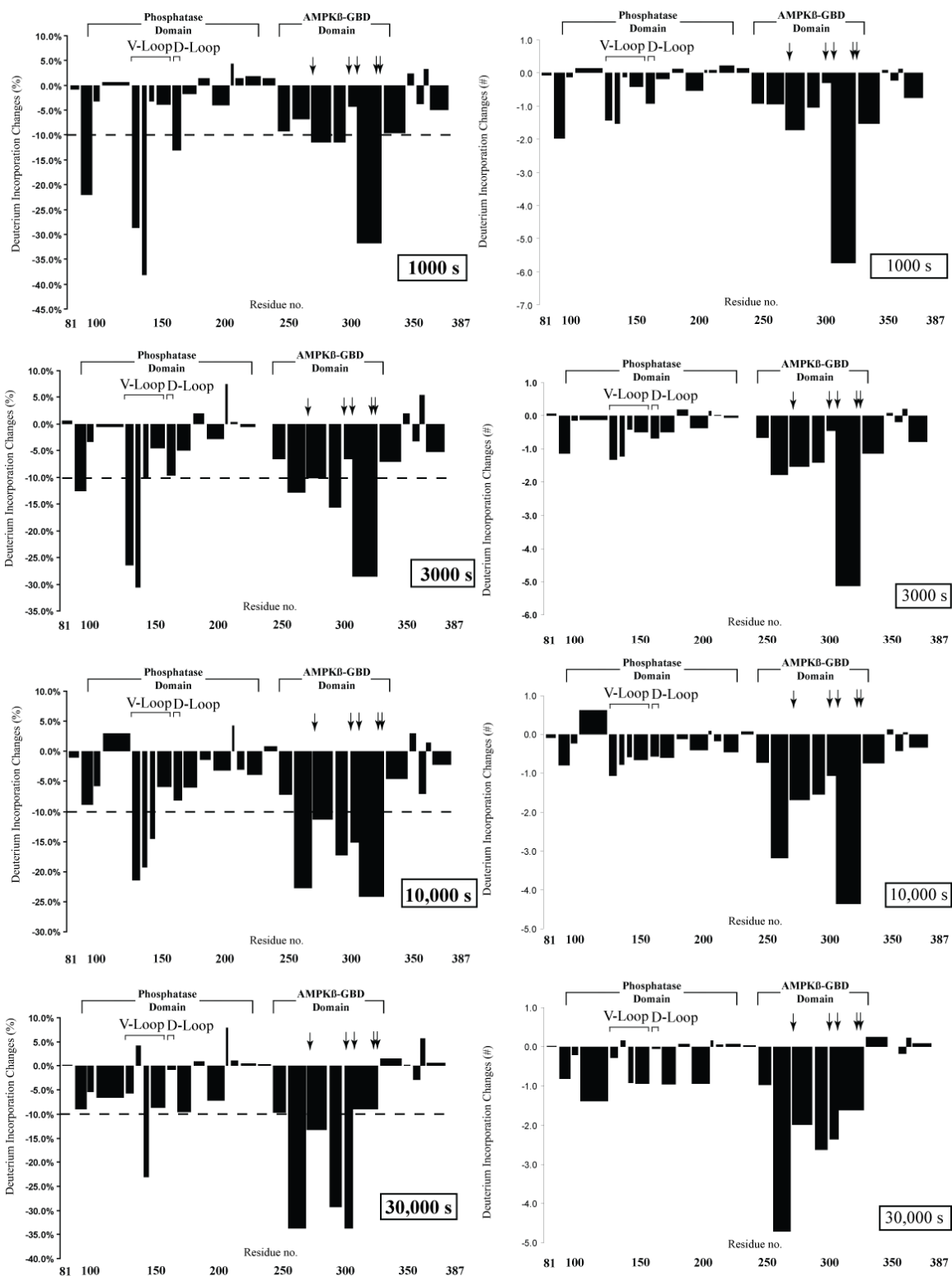
Supplemental Figure 1, Continued.



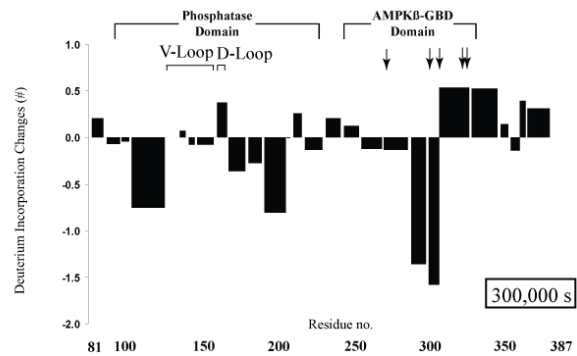
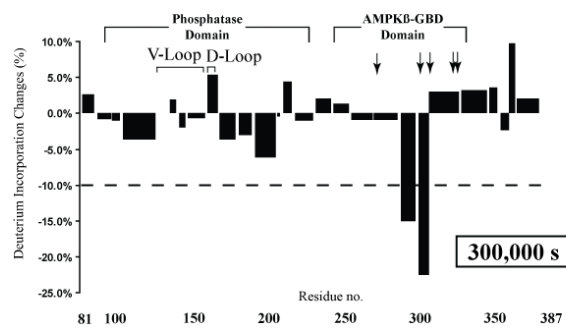
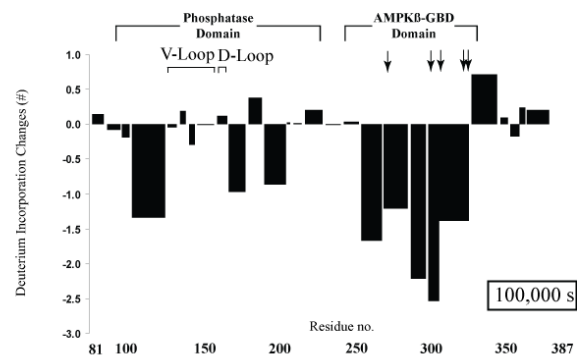
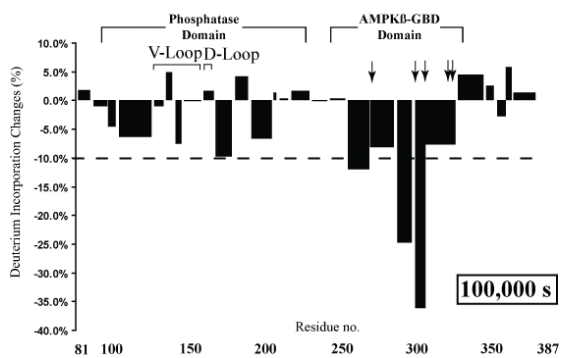
Supplemental Figure 2. Deuterium incorporation changes upon amylopectin binding. Corresponding time points (10 s, 100 s, 300 s, 1000 s, 3000 s, 10,000 s, 30,000 s, 100,000 s, 300,000 s) are shown boxed in the bottom right-hand corner of each plot. Two plots per time point are shown, one each for percent deuteration (left) and number deuterons (right). Plots labeled “Max” are composites of the residues that showed the greatest negative change at any time point. Changes greater than 10% (dotted line) are considered significant. V-loop = Variable loop. Arrows indicate putative key carbohydrate binding residues (from left to right: W278, K307, W314, G329, N333)



Supplemental Figure 2, Continued.



Supplemental Figure 2, Continued.



REFERENCES

- ¹ Wintrode PL, Tsutsui Y. Hydrogen/deuterium exchange and mass spectrometry: a powerful tool for probing protein structure, dynamics and interactions. *Curr. Med. Chem.* 2007;14:2344-2358.
- ² Lanman J, Lam TT, Barnes S, Sakalian M, Emmett MR, Marshall AG, Prevelige, Jr. PE. Identification of novel interactions in HIV-1 capsid protein assembly by high-resolution mass spectrometry. *J. Mol. Biol.* 2003; 325:759-772.
- ³ Lam TT, Lanman JK, Emmett MR, Hendrickson CL, Marshall AG, Prevelige, Jr. PE. Mapping of protein:protein contact surfaces by hydrogen/deuterium exchange, followed by on-line high-performance liquid chromatography electrospray ionization Fourier-transform ion-cyclotron-resonance mass analysis. *J. Chromatogr. A.* 2002; 982:85-95.
- ⁴ Turner BJ, Maurer M. Evaluating the roles of thrombin and calcium in the activation of coagulation factor XIII using H/D exchange and MALDI-TOF MS. *Biochemistry.* 2002; 41:7947-7954.
- ⁵ Mandell JG, Baerga-Ortiz A, Akashi S, Takio K, Komives EA. Solvent accessibility of the thrombin-thrombomodulin interface. *J. Mol. Bio.* 2001, 306:575-589.
- ⁶ Hsu YH, Burke JE, Stephens DL, Deems RA, Li S, Asmus KM, Woods, Jr. VL, Dennis EA. Calcium binding rigidifies the C2 domain and the intradomain interaction of GIVA phospholipase A2 as revealed by hydrogen/deuterium exchange mass spectrometry. *J. Biol. Chem.* 2008; 283:9820-9827
- ⁷ Burke JE, Hsu YH, Deems RA, Li S, Woods, Jr. VL, Dennis EA. A Phospholipid substrate molecule residing in the membrane surface mediates opening of the lid region in group IVA cytosolic phospholipase A₂. *J. Biol.Chem.* 2008; ahead of print.
- ⁸ Tsutsui Y, Wintrode PL. Hydrogen/deuterium exchange-mass spectrometry: a powerful tool for probing protein structure, dynamics and interactions. *Curr. Med. Chem.* 2007;14:2344-2358.
- ⁹ *Protein Folding, Dynamics, and Structural Evolution.* In *Biochemistry.* Second Edition Voet D, Voet JG., pp. 205-208. John Wiley and Sons, Inc., Somerset, New Jersey, USA, 1995.
- ¹⁰ Englander SW, Mayne L, Bai Y, Sosnick TR. Hyd Hydrogen exchange: the modern legacy of Linderstrøm-Lang. *Protein Science.* 1997;6:1101-1109.

- ¹¹ Wintrode PL, Friedrich KL, Vierling E, Smith JB, Smith DL. Solution structure and dynamics of a heat shock protein assembly probed by hydrogen exchange and mass spectrometry. *Biochemistry*. 2003;42:10667-10673.
- ¹² Englander SW, Sosnick TR, Englander JJ, Mayne L. Mechanisms and uses of hydrogen exchange. *Curr. Opin. Struct. Biol.* 1996;6:18-23.
- ¹³ Ianzano L, Jang J, Chan EM, Zhao XC, Lohi H, Scherer SW, Minassian BA. Lafora progressive myoclonus epilepsy mutation database-EPM2A and NHLRC1 (EPM2B) genes. *Hum. Mutat.* 2005;26:397.
- ¹⁴ Collins GH, Cowden RR, Nevis AH. Myoclonus epilepsy with Lafora bodies. An ultrastructural and cytochemical study. *Arch. Pathol.* 1968;86:239-254.
- ¹⁵ Harriman DG, Millar JH, Stevenson AC. Progressive familial myoclonic epilepsy in three families: its clinical features and pathological basis. *Brain*. 1955;78:325-349.
- ¹⁶ Carpenter S, Karpati G. Sweat gland duct cells in Lafora disease: diagnosis by skin biopsy. *Neurology*. 1981;31:1564-1568.
- ¹⁷ Gentry MS, Downen III RH, Worby CA, Mattoo S, Ecker JR, Dixon JE. The phosphatase laforin crosses evolutionary boundaries and links carbohydrate metabolism to neuronal disease. *J. Cell Biol.* 2007;178:477-488.
- ¹⁸ Myers MP, Stolarov JP, Eng C, Li J, Wang SI, Wigler MH, Parsons R, Tonks NK. P-TEN, the tumor suppressor from human chromosome 10q23, is a dual-specificity phosphatase. *PNAS*. 1997;94:9052-0957.
- ¹⁹ Worby CA, Gentry MS, Dixon JE. Laforin, a dual specificity phosphatase that dephosphorylates complex carbohydrates. *J. Biol. Chem.* 2006;281:30412-30418.
- ²⁰ Tagliabracci VS, Turnbull J, Wang W, Girard JM, Zhao X, Skurat AV, Delgado-Escueta AV, Minassian BA, Depaoli-Roach AA, Roach PJ. Laforin is a glycogen phosphatase, deficiency of which leads to elevated phosphorylation of glycogen *in vivo*. *PNAS*. 2007;104:19262-19266.
- ²¹ Yokoi S, Austin J, Witmer F. Isolation and characterization of Lafora bodies in two cases of myoclonus epilepsy. *J. Neuropathol. Exp. Neurol.* 1967;26:125-127.
- ²² Sakai M, Austin J, Witmer F, Trueb L. Studies in myoclonus epilepsy (Laforin body form): II. Polyglucosans in the systemic deposits of myoclonus epilepsy and in corpora amylacea. *Neurol.* 1970;20:160-176.

- ²³ Schnabel R, Seitelberger F. Histophysical and histochemical investigations of myoclonus bodies. *Pathol. Eur.* 1968;3:218-226.
- ²⁴ Yokoi S, Austin J, Witmer F, Sakai M. Studies in myoclonus epilepsy (Lafora body form). I. Isolation and preliminary characterization of Lafora bodies in two cases. *Arch. Neurol.* 1968;19:15-33.
- ²⁵ Blennow A, Nielsen TH, Baunsgaard L, Mikkelsen R, Engelsen SB. Starch phosphorylation: a new front line in starch research. *Trends Plant Sci.* 2002;7:445-450.
- ²⁶ Smith AM, Zeeman SC, Smith SM. Starch degradation. *Annu. Rev. Plant Biol.* 2005;56:73-98.
- ²⁷ Zeeman SC, Smith SM, Smith AM. The diurnal metabolism of leaf starch. *Biochem. J.* 2007;401:13-28.
- ²⁸ Polekhina G, Gupta A, van Denderen BJ, Feil SC, Kemp BE, Stapleton D, Parker MW. Structural basis for glycogen recognition by AMP-activated protein kinase. *Structure.* 2008;13:1453-1462.
- ²⁹ Das S, Cho W. Roles of catalytic domain residues in interfacial binding and activation of group IV cytosolic phospholipase A₂. *J. Biol. Chem.* 2002;277:23838-23846.
- ³⁰ Mandell JG, Falick AM, Komives EA. Identification of protein-protein interfaces by decreased amide proton solvent accessibility. *PNAS.* 1998;95:14705-14710.
- ³¹ Hoofnagle AN, Resing KA, Goldsmith EJ, Ahn NG. Changes in protein conformational mobility upon activation of extracellular regulated protein kinase-2 as detected by hydrogen exchange. *PNAS.* 2001;98:956-961.
- ³² Brudler R, Gessner CR, Li S, Tyndall S, Getzoff ED, Woods, Jr. VL. PAS domain allostery and light-induced conformational changes in photoactive yellow protein upon I₂ intermediate formation, probed with enhanced hydrogen/deuterium exchange mass spectrometry. *J. Mol. Biol.* 2006;363:148-160.
- ³³ Hochrein JM, Lerner EC, Schiavone AP, Smithgall TE, Engen JR. An examination of dynamics crosstalk between SH2 and SH3 domains by hydrogen/deuterium exchange and mass spectrometry. *Prot. Sci.* 2006;15:65-73.
- ³⁴ Zhang Z, Smith DL. Determination of amide exchange by mass spectrometry: A new tool for protein structure elucidation. *Prot. Sci.* 1993;2:522-531.
- ³⁵ Denu J, Dixon JE. Protein tyrosine phosphatases: mechanisms of catalysis and regulation. *Curr. Opin. Chem. Biol.* 1998;5:633-641.

- ³⁶ Polekhina G, Gupta A, van Denderen BJ, Feil SC, Kemp BE, Stapleton D, Parker MW. Structural basis for glycogen recognition by AMP-activated protein kinase. *Structure*. 2005;13:1453-1462.
- ³⁷ Polekhina G, Gupta A, Michell BJ, van Denderen B, Murthy S, Feil SC, Jennings IG, Campbell DJ, Witters LA, Parker MW, et al. AMPK beta subunit targets metabolic stress sensing to glycogen. *Curr Biol*. 2003;13:867-871.
- ³⁸ Borason AB, Bolam DN, Gilbert HJ, Daview GJ. Carbohydrate-binding modules: fine-tuning polysaccharide recognition. *Biochem. J*. 2004;382:769-781.
- ³⁹ Begley MJ, Taylor GS, Brock MA, Ghosh P, Woods VL, Dixon JE. Molecular basis for substrate recognition by MTMR2, a myotubularin family phosphoinositide phosphatase. *PNAS*. 2006; 103:927-932.
- ⁴⁰ Maehama T, Dixon JE. The tumor suppressor, PTEN/MMAC1, dephosphorylates the lipid second messenger, phosphatidylinositol 3,4,5-trisphosphate. *J. Biol. Chem*. 1998;273:13375-13378.
- ⁴¹ Lee J, Yang H, Georgescu M, Cristofano AD, Maehama T, Shi Y, Dixon JE, Pandolfi P, Pavletich NP. Crystal structure of the PTEN tumor suppressor: implications for its phosphoinositide phosphatase activity and membrane association. *Cell*. 1999;99:323-334.
- ⁴² Alonso A, Rojas A, Godzik A, Mustelin T. The dual-specific protein tyrosine phosphatase family. *Topics in Curr. Genetics*. 2004;5:333-352.
- ⁴³ Woods, Jr. VL, Hamuro Y. High resolution, high-throughput amide deuterium exchange-mass spectrometry (DXMS) determination of protein binding site structure and dynamics: utility in pharmaceutical design. *J. Cell Biol*. 2001; 37:89-98.
- ⁴⁴ Molday RS, Englander SW, Kallen RG. Primary structure effects on peptide group hydrogen exchange. *Biochemistry*. 1972;11:150-158.
- ⁴⁵ Bai Y, Milne JS, Mayne L, Englander SW. Primary structure effects on peptide group hydrogen exchange. *Proteins: Structure, Function, and Genetics*. 1993;17:75-86.